AL.2.1992-297
C.2

CANADIANA
JUN 29 1992

EVALUATION OF FLASH FIRE PROTECTIVE CLOTHING USING AN INSTRUMENTED MANNEQUIN

A PROJECT FUNDED BY THE
OCCUPATIONAL HEALTH AND SAFETY
HERITAGE GRANT PROGRAM

[redacted]

EVALUATION OF FLASH FIRE PROTECTIVE CLOTHING USING AN INSTRUMENTED MANNEQUIN

EVALUATION OF FLASH FIRE PROTECTIVE CLOTHING USING AN INSTRUMENTED MANNEQUIN

Final Research Project Report
Prepared for
Alberta Occupational Health and Safety
Heritage Grant Program

By

E.M. Crown[1], Ph.D.
J.D. Dale[2], Ph.D.

[1]Department of Clothing and Textiles
[2]Department of Mechanical Engineering
University of Alberta
Edmonton, Alberta, Canada

March 30, 1992

Digitized by the Internet Archive
in 2016

https://archive.org/details/evaluationofflas00crow

TABLE OF CONTENTS

EXECUTIVE SUMMARY v

ACKNOWLEDGEMENTS vi

A. INTRODUCTION 1

B. EXPERIMENTAL SYSTEM AND METHOD OF EVALUATION 2
- FLASH FIRE GENERATION SYSTEM AND FIRING ROOM 9
- DATA ACQUISITION SYSTEM 13
- SKIN DAMAGE EVALUATION 14
- HEAT TRANSFER MODEL OF HUMAN SKIN 16

C. GARMENT TESTING WITH VARIED EXPOSURES 19

RESULTS 21

D. SUMMARY AND CONCLUSIONS 29
- REFERENCES 30

APPENDIX 31

LIST OF TABLES

TABLE 1 Thermal Properties of Human Skin and Skin Simulant 7

TABLE 2 Parameters Used in Numerical Model of Human Skin 17

TABLE 3 Fabric Characterization and Thermal Protective Performance Ratings of Fabrics Used in Garments Tested 20

TABLE 4 Percent of Mannequin Surface Reaching 2nd or 3rd-Degree Burn Criteria 22

TABLE A1 Thermal Properties of Human Skin and Skin Simulant 43

TABLE A2 Parameters Used in the Model 62

TABLE A3 The numbers of grids, stretching ratios and time-steps used for testing the model 64

TABLE A4 Comparison of the Finite Difference and Analytical Solutions for a Transient Temperature Problem 65

TABLE A5 The Parameters Used in the Three Versions 69

LIST OF FIGURES

Fig. 1 Front and rear views of instrumented mannequin 3

Fig. 2 Skin simulant sensor 6

Fig. 3 Sensor areas on instrumented mannequin 8

Fig. 4 Flash fire burner system 10

Fig. 5 Layout of flash fire room 12

Fig. 6 Human skin tolerance time to absorbed energy showing calibration points obtained using a calibrated heat flux source on a skin simulant sensor 18

Fig. 7 Mean percent mannequin surface reaching 2nd or 3rd degree burn criteria 23

Fig. 8 Calculated location of skin burning on mannequin Garment B, 75 kW/m^2, 3 second exposure 24

Fig. 9 Calculated location of skin burning on mannequin Garment B, 75 kW/m^2, 4 second exposure 25

Fig. 10 Calculated location of skin burning on mannequin Garment E, 75 kW/m^2, 3 second exposure 26

Fig. 11 Calculated location of skin burning on mannequin Garment E, 75 kW/m^2, 4 second exposure 27

Fig. 12 Calculated cumulative skin burning for a typical 4 second exposure with protective clothing 28

Fig. A1 The flow diagram of the program 32

Fig. A2 Calibration result of the thermal inertia of a skin simulant sensor 44

Fig. A3 Variation of the thermal inertia of the 110 skin simulants 45

Fig. A4a The skin model 49

Fig. A4b The volume element of skin indicating the blood flow (solid arrows) and heat transfer (dotted arrows) 50

Fig. A5 A nonlinear finite difference grid for the skin model 53

Fig. A6 Measured and predicted human skin tolerance time to absorbed energy rate . . . 70

EXECUTIVE SUMMARY

The purpose of this project was to refine and further develop an instrumented mannequin/flash fire exposure system developed in an earlier project, and to use the system to study the effect of several variables on the measured protective qualities of various protective garments. This report describes the results obtained.

The number of skin simulant sensors in the mannequin was increased from 80 to 110, and the computer controlled data acquisition system modified to accept the additional 30 input channels. In addition, the computer codes were modified to record and store the additional data. To produce more accurate skin burn predictions, the thermal conductivity of the skin simulant material was measured with a special instrument at the National Research Council of Canada. The measured value was about 100% larger than the value used previously.

The mannequin/flash fire system was installed in a new facility dedicated for this purpose. Additional burners and gas storage capacity were added to the flash fire generating system. This permitted steadier gas flows and more uniform heat flux exposure to the mannequin surface. The repeatability in the predicted surface area of the mannequin receiving second degree burns or worse is better than 95% for average heat fluxes up to 84 kW/m^2 and up to 4 seconds duration.

Testing of representative garments showed that the effects of varying heat flux and exposure times differs with garment type, and that while the TPP test results showed similar trends, the TPP results did not predict the behaviour of all of the garments tested on the mannequin. It is suggested that whenever possible, the exposure conditions for mannequin testing should be selected to most closely simulate the hazardous environment form which protection is sought.

ACKNOWLEDGEMENTS

Financial support for this project from the Alberta Occupational Health and Safety Heritage Grant Program is gratefully acknowledged. Additional financial support for this project from the Natural Sciences and Engineering Research Council of Canada and the Canadian Petroleum Association is gratefully acknowledged. The authors also acknowledge with thanks the cooperation of Todd Canada Inc. (formerly S.C. Walker Manufacturing Company Limited), Safety Supply Canada, Workrite, Hoeschst Celanese, Westex Inc., Dominion Textiles and Dominion Industrial Fabrics for supplying garments or fabrics for this research. We also thank Mark Ackerman, Elaine Bitner, Dr. Kathy Rigakis and Yi-bin Tan for assistance in conducting the experiments.

A. INTRODUCTION

In many industrial settings workers potentially can be exposed to flash fires and fireballs. The oil and gas and petrochemical industries are ones where ignition of gas leaks can produce accidents resulting in injury and loss of life through skin burns. Investigation of numerous accidents suggest that workers can be exposed to intense heat flux ($\approx$ 80 kW/m^2) for relatively short periods of time, typically five seconds or less. While protective clothing is available for use in these potentially hazardous environments, evaluation of such clothing typically has been through small scale laboratory tests of flame resistance and thermal protective performance. Although such tests may give valuable information about the fabrics used in thermal protective clothing, they do not necessarily predict how well garments or garment assemblies will perform when actually exposed to a flash fire.

One method of evaluating protective garments is to expose a clothed instrumented mannequin to a controlled flash fire and to assess the resulting potential skin damage. The potential skin damage can be evaluated using computer models if the local heat flux to the surface is known. If the heat flux and exposure time can be varied reliably, then different accident scenarios can be simulated. The problem addressed by this research was the refinement and further development of an instrumented mannequin/flash fire exposure system developed in an earlier project, "Systematic Assessment of Protective Clothing for Alberta Workers" [1]. This is the only mannequin of its type in Canada and one of the few world-wide. The purpose of the system is to assist industry in assessing the protective qualities of garment systems when subjected to flash fires of varying duration and intensity, by estimating potential for skin burn damage.

The system as originally developed was limited in its uniformity of exposure and range of heat flux. In addition, the estimation of potential for skin damage is directly dependent upon knowing the thermal-physical properties of the skin simulant sensors. Thus, accurate measurement of these properties is required to obtain the best possible estimates. The **purpose** of this research was (a) to develop and refine an instrumented mannequin and flash fire exposure system, and (b) to determine the effect of varying heat flux and exposure time on the measured protective properties of several protective garments. Specific **objectives** were:

(a) to modify the flash fire generation system to provide both (i) controlled variation of heat flux, and (ii) uniform exposure;

(b) to measure the thermal-physical properties of the skin simulant material;

(c) to add more skin simulant sensors to more thoroughly cover the mannequin as well as additional data acquisition capability;

(d) to modify the computer code to speed calculations and provide better graphical portrayal of skin damaged areas; and

(e) to test various garment systems at varied heat fluxes and exposure times.

The remainder of the report is divided into two main sections. The first section covers objectives (a) to (d), relating to the refinement of the mannequin and flash fire exposure systems. The second section reports on the experiments in which heat flux and exposure time were varied. A brief section on interlaboratory testing follows. A final section includes a summary of the project and our conclusions.

B. EXPERIMENTAL SYSTEM AND METHOD OF EVALUATION

The male mannequin, size 40R, was constructed out of fibreglass by duplicating the shape of an existing store mannequin. This was done using female-male molding techniques. Hand lay up of matting and resin was used to produce a 3 mm thick shell. This thickness of fibreglass was used in order to provide sufficient strength for handling and to have a thick enough layer for easy mounting of heat flux sensors. Before construction, samples of hardened fibreglass were exposed to large flash fires at a fire fighting school to ensure suitability.

Figure 1 shows the front and rear views of the mannequin. A lift out panel was designed into the chest area to facilitate the installation of the heat flux sensors and their wiring. The output cable from all the sensors is fed out of the mannequin through a ten cm diameter aluminum pipe molded into the head. A steel cable wrapped around this pipe is used to hang the mannequin. Note that the mannequin exhibits large muscle groups typical of those found on a well conditioned adult male. The arms and hands are removable to facilitate dressing. Mounting sockets were molded into the shoulders and forearms for this purpose. The hands are solid fibreglass.

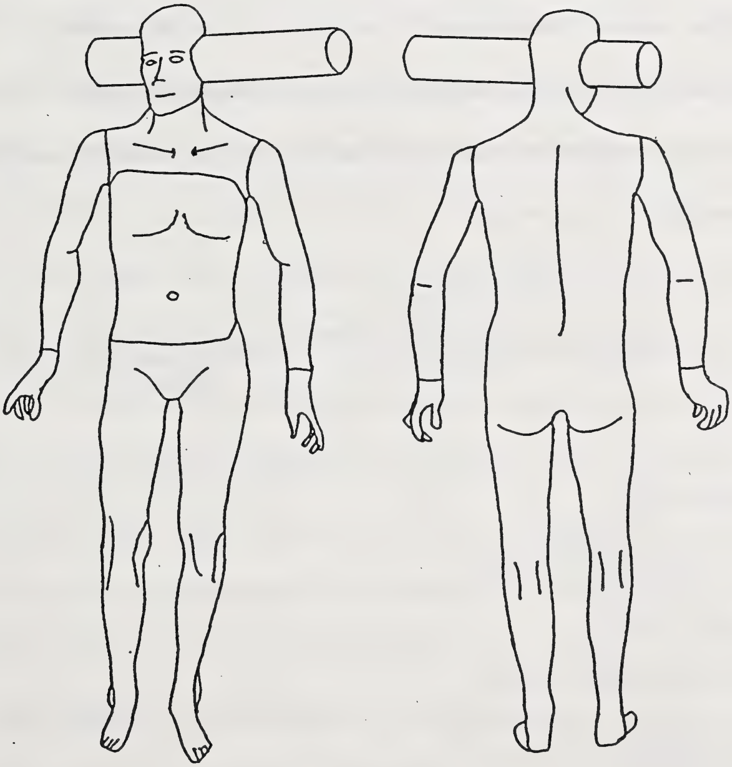

Fig. 1 Front and rear views of instrumented mannequin

Heat Flux Sensors

The thermal protective quality of a garment is judged on estimates of the extent of skin damage resulting from a controlled flash fire. In order to estimate the skin damage, the heat transfer to the surface of the mannequin needs to be measured. Once the heat transfer and its variation with location and time is known, a heat transfer model of human skin can be used to estimate the damage due to burning. The heat flux sensors (skin simulant sensors) used in the mannequin should ideally be as close as possible to human skin in their response to the heat transfer. This minimizes the corrections that have to be applied in the model.

Heat transfer from a short duration flash fire into the surface of the mannequin (or the skin of a human) can be modelled as transient heat transfer into a semi-infinite slab. For the case of a constant heat flux at the surface and constant thermal physical properties the analytical solution can be shown to be [2]

$$T(x,t) - T_i = \frac{q}{k}\left[2\sqrt{\frac{\alpha t}{\pi}}\, e^{-\frac{x^2}{4\alpha t}} - x\,\mathrm{erfc}\left(\frac{x}{2\sqrt{\alpha t}}\right)\right] \tag{1}$$

Where:

T = temperature, K

T_i = initial temperature in slab, K

q = heat flux, W/m^2

k = thermal conductivity, W/m· K

α = thermal diffusivity ($k/\rho c$), m^2/s

ρ = density, kg/m^3

c = specific heat, J/kg·°C

t = time, s

e = 2.7183

x = distance into slab, m

erfc = complimentary error function

At the surface (i.e. x = 0) this reduces to

$$T(0,t) - T_i = \frac{2q\sqrt{t}}{\sqrt{\pi k \rho c}} \tag{2}$$

This latter form illustrates that the product kρc, the thermal inertia, or its square root, the thermal absorptivity, is the grouping of thermal physical properties that should be matched between the heat flux sensors and human skin.

The design selected for the skin simulant sensors is shown in Fig. 2. The material "Colorceran" is commonly used to form the top layer of chemistry laboratory benches. The thermal physical properties of this material, at least as far as its ability to simulate the short duration heat transfer from a flash fire into human skin is concerned, are close to ideal. Table 1 lists values of the thermal physical properties of the two outer layers of human skin, that is the epidermis and dermis layers, and those of Colorceran. While the individual properties are not a perfect match with those of the epidermis and dermis layers, the product kρc, or its square root, are closely matched. The thermal physical properties for human skin listed in Table 1 were taken from the literature [3,4].

The shape of the skin simulant sensors was selected for convenience. The Colorceran comes in 32 mm thick slabs. The 19 mm diameter was selected to give a large enough diameter so that sufficient lead length could be given to the thermocouple on the surface to reduce conduction heat transfer effects to the junction. A hole was drilled along the long axis of the sensor to allow the thermocouple wire to be run into the inside of the mannequin. The thermocouple wire used was 30 gauge copper constantan. The section on the surface of the sensor was rolled flat, approximately 0.1 mm thick, prior to installation. The wire is held on to the surface of the sensor with a special high temperature epoxy-phenolic adhesive. The adhesive has a maximum short term working temperature of 370°C, which was thought to be well above the surface temperatures reached in the short duration flash fires. To date no sensor failures have occurred due to the adhesive losing its bond.

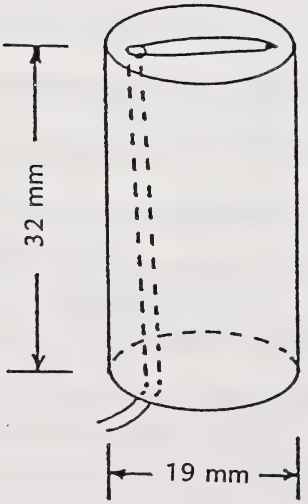

30 gauge Cu-Co wire, rolled flat ~ 0.1 mm thick held on surface with an epoxy-phenolic adhesive.

"Colerceran" - inorganic mixture of calcium, aluminum, silicate with asbestos fibres and a binder.

Fig. 2 Skin simulant sensor

TABLE 1 Thermal Properties of Human Skin and Skin Simulant

Property	Human Skin		Skin Simulant
	Epidermis	Dermis	
k (W/m· K)	0.255	0.523	0.97
ρ (kg/m^3)	1200	1200	1877
c (J/kg·K)	3598	3222	1205
$k\rho c$ (J^2/m^4 · °C^2 · s)	1.1×10^6	2.0×10^6	2.2×10^6
$\sqrt{k\rho c}$ (J/m^2 · °C · s$^{1/2}$)	1050	1414	1483

To adequately cover the mannequin, 110 sensors were used. Each sensor was mounted as flush as possible with the fibreglass exterior of the mannequin by drilling a hole in the shell and gluing the sensor in place with fibreglass resin. The sensors can be removed by cutting the resin bond. The distribution of the sensors is shown in Fig. 3, approximately one per unit surface area. None are mounted in the lower arms (wrist region), hands or feet below the ankles. After the sensors were installed, the entire mannequin surface was painted with flat black high temperature paint. This paint has a rated temperature of 600°C.

The thermocouple wire from each sensor is positioned inside the mannequin to terminate on a juncton board located in the chest cavity. About 15 m of copper wire is used to connect each thermocouple to the data acquisition system. The extension wire exits the mannequin through the aluminum tube molded into its head. An aluminum foil radiation shield is used to protect the exposed extension wire from the flash fires.

Each sensor was calibrated in situ using a 380 W movie projector lamp powered by a variable voltage power supply. The lamp output was calibrated with three slug calorimeters so that its radiant heat flux was known to within a few percent. However, the calibration accuracy with

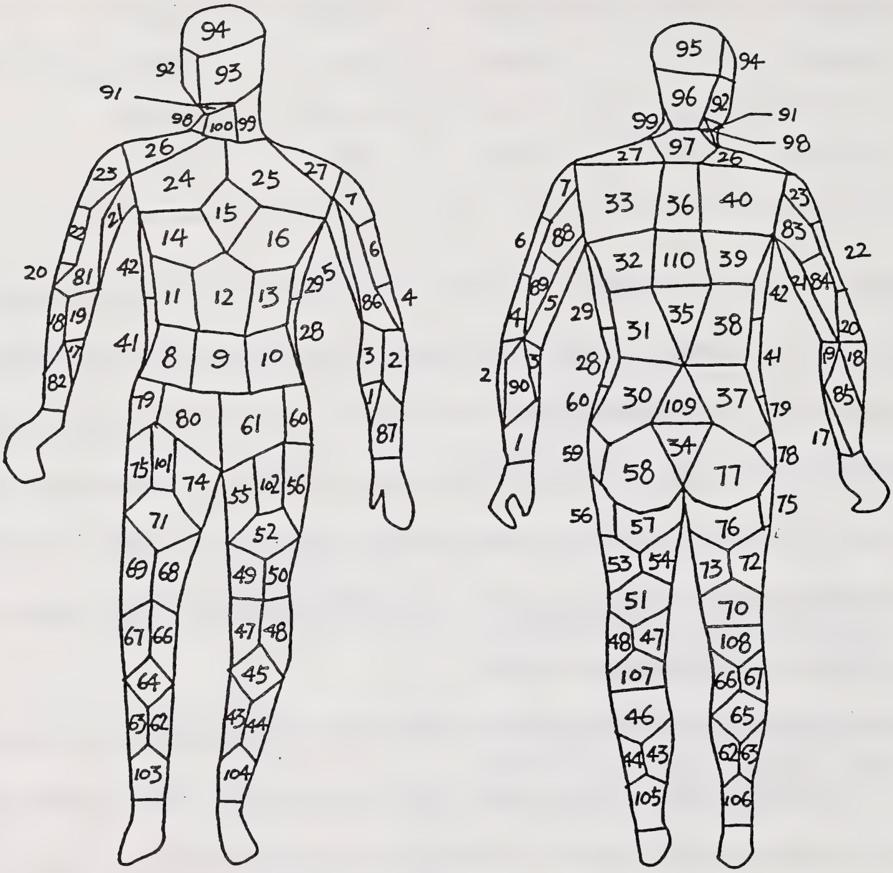

Fig. 3 Sensor areas on instrumented mannequin

the movie projector lamp is limited because it does not produce a perfectly uniform heat flux on the surface of the sensor.

The thermal absorptivity of each sensor was determined from data collected during the calibration process. The specific value measured for each sensor was stored in the computer controlled data acquisition system and is used whenever heat transfer data is collected during a flash fire. Calibration of the 110 sensors showed that the mean value of the thermal absorptivity was within 7% of the value listed in Table 1, and that the standard deviation for the sample was less than 10% of the mean. A histogram of the sensor calibration is included in the Appendix. The thermal absorptivity value listed in Table 1 was calculated from measured thermal physical properties of the sensor material. These measurements were made by the Institute for Research in Construction, National Research Council of Canada.

FLASH FIRE GENERATION SYSTEM AND FIRING ROOM

The flash fires are generated with propane diffusion flames. Six identical burner assemblies, positioned around the mannequin, are used. Each burner assembly, Fig. 4, consists of two "tiger torches" supplied with propane at three atmospheres absolute pressure. The air mixing nozzles in the burner heads were removed and flow control orifices installed upstream. Interchangeable orifices are used to set the mass flow rate of fuel through each burner. The three atmosphere gas pressure was selected to produce choked flow in the orifices. This permits the average heat flux to be varied from about 67 kW/m^2 to 84 kW/m^2 (1.6 $cal/cm^2 \cdot sec$ to 2.0 $cal/cm^2 \cdot sec$). Electric solenoid valves are used to turn on and off the gas flow to the burners. The duration of the burn is programmed through the data acquisition system. Pilot lights are used to ignite the main gas flow exiting each burner.

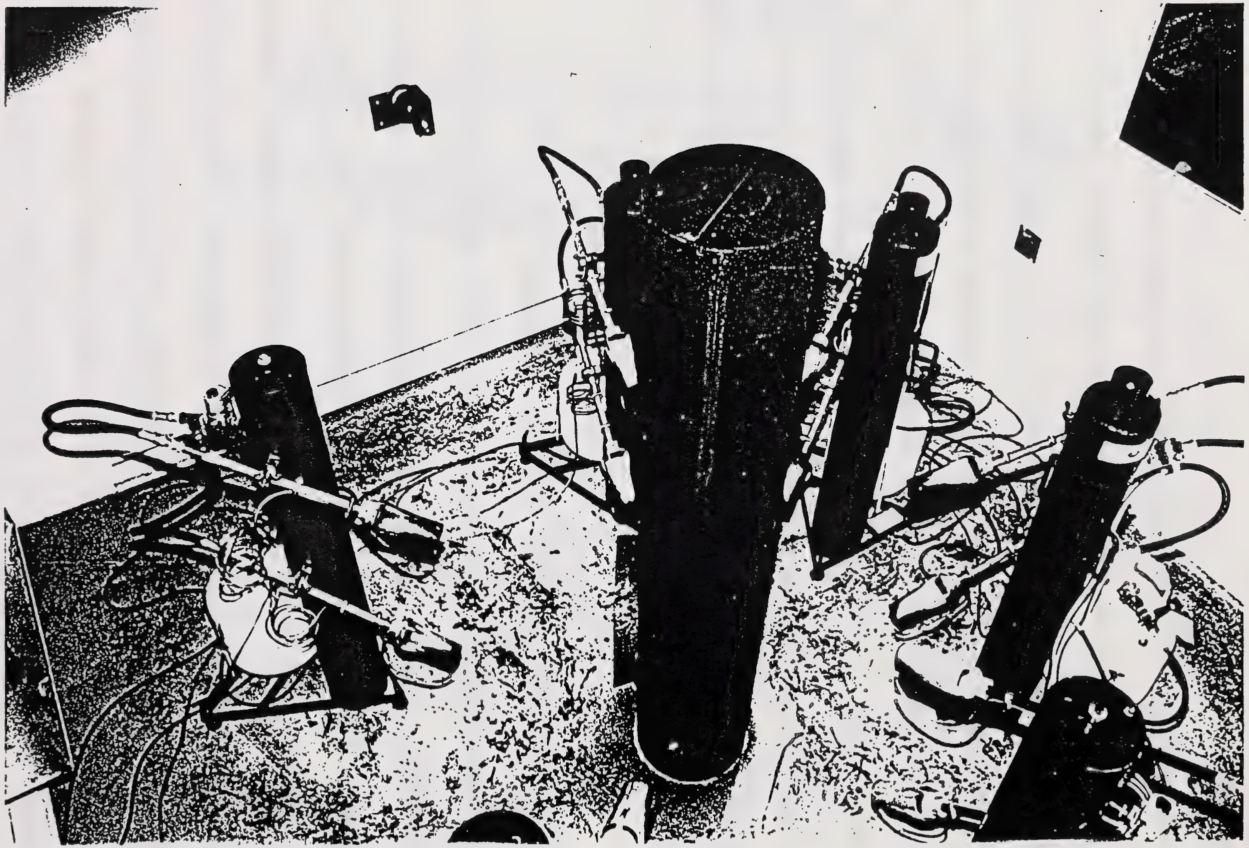

Fig. 4 Flash fire burner system

The average heat flux was determined by direct measurement. The nude mannequin was subjected to either a three or four second flash fire and for each skin simulant sensor the instantaneous heat flux calculated at one second intervals. The mean, maximum, minimum and standard deviation were then calculated from the data set. The mean was then taken to be the average heat flux when testing garments at the same settings. To illustrate values, a typical 3 second exposure would produce maximum and minimum values of 160 kW/m^2 and 48 kW/m^2, respectively with a mean of 79 kW/m^2 and a standard deviation of 22 kW/m^2 based on all 110 sensors.

The flash firing system is housed in a special concrete block room added on to the Mechanical Engineering Acoustics and Noise Unit, a facility operated by the Department of Mechanical Engineering, University of Alberta. The room, Fig. 5, is approximately 4 m by 4 m in plan, and 4 m high. It is fitted with two remote controlled dampers for fresh air supply during firing and venting. The size of each damper is approximately 0.5 m × 0.75 m. Venting of gases is done after firing via a fan located in the ceiling of the room. A 1.5 m by 1 m viewing window made of wire reinforced glass is located in the wall that separates the firing room from the main laboratory building. As indicated in Fig. 5, the six burner assemblies are located in the room so as to produce as uniform heat flux on the surface of the mannequin as possible. The six burner assemblies are fed from four 0.1 m^3 gaseous propane cylinders set in the corners of the room. The four tanks are connected by steel pipe to one another and to a 0.1 m^3 liquid propane storage bottle located outside the room. This latter bottle is fitted with a pressure regulator for setting the gas storage pressure in the firing room.

The burner system is prevented from accidental firing through safety lockouts. These include a thermocouple based pilot flame sensor system, one for each burner head, and a normally closed solenoid valve used to isolate the outside liquid propane storage system from the inside vapour storage containers. Only when the outside tank is isolated and all the pilot lights are burning will the computer-data acquisition system permit a signal to be sent to start the gas flow to the burner heads.

With the system as shown in Fig. 5, only a 11% drop in mass flow rate occurs during a three second firing. A ten second firing produces a 25% decrease in mass flow rate from beginning to end.

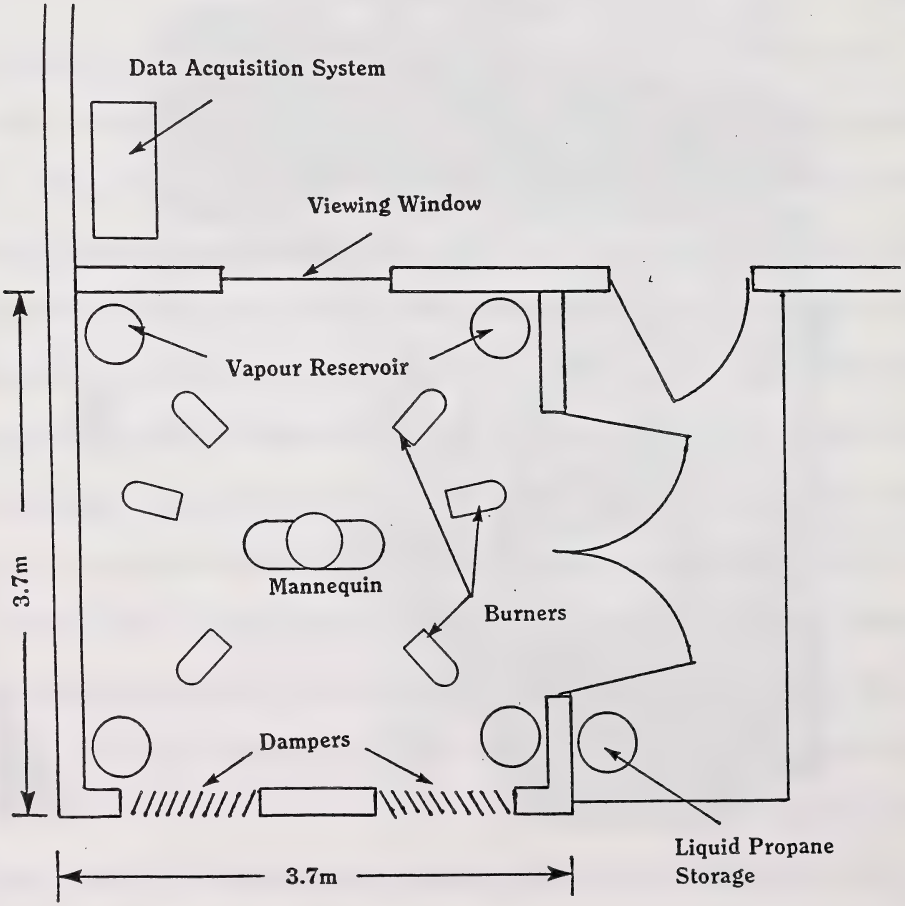

Fig. 5 Layout of flash fire room

DATA ACQUISITION SYSTEM

A computer controlled data acquisition system is used to run the tests, record and store data, and to calculate and display the results of the numerical model used to estimate the skin damage. The output from the 110 thermocouples on the skin simulant sensors is first fed into an analog amplifier multiplexer, the output being amplified 200 times. This amplified output is then fed into a 12 bit analogue-to-digital convertor mounted inside the computer. The digitized signals are written either directly into a temporary memory or permanent storage by writing directly to a disk. The conversion rate for the analogue to digital converter is up to 800 Hz, thus each of the 110 thermocouples can be read about eight times a second. With a 12 bit system the signal resolution is 1 part in 4096, while the 800 Hz sampling rate produces a timing error of about 0.125 seconds for any thermocouple.

To run an experiment, software specially written for this purpose is first loaded into the computer. It prompts the user for information about the test such as the burn duration and total data sample time. Once this is keyed in, the computer system checks that the pilot lights for the burners are lit and waits for a start signal. After receiving a start signal the unit displays all 110 temperatures of the sensors. If these are satisfactory, for example not more than 25°C, a run signal is given by the operator. The system then takes zero readings from all 110 sensors and turns on the burners for the prescribed time. Sampling during firing is done at 800 Hz during burner on times and then continues at 110 Hz for a maximum of two minutes. Once sampling is finished the temperature data is loaded into a file for later use.

SKIN DAMAGE EVALUATION

The purpose of the protective clothing is to prevent skin damage when exposed to a flash fire. Skin damage is usually identified as being first, second or third degree burn. For this study only second degree or worse is of importance.

Many investigators have examined skin burning and developed criteria to predict when irreversible damage begins [5-9]. Damage begins when the growing or basal layer has its temperature raised above 44°C. At this temperature irreversible damage begins to occur to the basal layer and the longer it is at or above this temperature the greater the amount of damage. Experiments on human and pig skin showed that the rate of destruction of the basal layer could be adequately described as a chemical reaction of the first order. The criterion used was suggested originally by Henriques [6] and is of the form

$$\frac{d\Omega}{dt} = P e^{-\frac{\Delta E}{RT}} \tag{3}$$

where

Ω = a quantitative measure of burn damage at the basal layer or at any depth in the dermis

P = frequency factor, s^{-1}

ΔE = the activation energy for skin, J/mole

R = the universal gas constant, 8.315 J/kmol·K

T = the absolute temperature at the basal layer or at any depth in the dermis, K

t = total time for which T is above 44°C (317.15 K)

The total burn damage is found by integrating equation (3) over the time interval that the basal layer is above 44°C. That is,

$$\Omega = \int_0^t P e^{-\frac{\Delta E}{RT}} dt \tag{4}$$

Henriques [6] found that if Ω is less than or equal to 0.5 no damage will occur at the basal layer. If Ω is between 0.5 and 1.0 first degree burns will occur, while if $\Omega > 1.0$ second degree burns will result. This total damage criteria can be applied to any depth of skin provided the appropriate values of P and ΔE are used.

Morse et al. [7] have examined the various values of P and ΔE available in the literature and suggests that the criteria developed by Stoll and co-workers [8,9] be used in the epidermal layer and that of Takata [10] be used in the dermal and subcutaneous layers. The values of P and ΔE developed by Stoll are:

$$\left.\begin{aligned} P &= 2.185 \times 10^{124}\ \text{sec}^{-1} \\ \Delta E/R &= 93{,}534.9\ K \end{aligned}\right\} \qquad for\ T < 50°C$$

$$\left.\begin{aligned} P &= 1.823 \times 10^{51}\ \text{sec}^{-1} \\ \Delta E/R &= 39{,}109.8\ K \end{aligned}\right\} \qquad for\ T \geq 50°C$$

while those of Takata are:

$$\left.\begin{aligned} P &= 4.32 \times 10^{64}\ \text{sec}^{-1} \\ \Delta E/R &= 50{,}000\ K \end{aligned}\right\} \qquad for\ T < 50°C$$

$$\left.\begin{aligned} P &= 9.39 \times 10^{104}\ \text{sec}^{-1} \\ \Delta E/R &= 80{,}000\ K \end{aligned}\right\} \qquad for\ T \geq 50°C$$

In order to predict the extent of damage that would result in a flash fire it is necessary to know the temperature history of the basal layer. The heat flux sensors in the mannequin are used for this purpose. They permit the surface heat flux and its variation with time to be predicted. This information is then used in a numerical model for heat transfer in human skin in order to predict the temperature history of the basal layer and the extent of skin damage for each of the 110 sensors. A full description of skin burn criteria can be found in the Appendix.

HEAT TRANSFER MODEL OF HUMAN SKIN

The skin model used is based on one developed by Metha and Wong [3]. This model divides the skin into three tissue layers, the epidermis, dermis, and subcutaneous, plus an isothermal core. It also allows for blood flow through arteries and veins to the epidermis-dermis interface. An energy balance on a region of skin containing both arteries, veins and capillaries produces,

$$c\rho \frac{\partial T}{\partial t} = k\frac{\partial^2 T}{\partial x^2} - (c\rho)_b G(T - T_b) \qquad (5)$$

where:

$(c\rho)_b$ = volumetric heat capacity of the blood, $J/m^3 \cdot K$

G = blood perfusion rate, $m^3/s/m^3$ of tissue volume

T_b = blood perfusion temperature, K (assumed equal to the internal body temperature, 310 K)

T = tissue temperature, K

and the other terms are as defined earlier.

This equation is solved numerically for each of the 110 sensors. The object is to predict the temperature distribution and history in the skin until no further damage occurs, or the entire thickness of the epidermis and dermis layers has an Ω value greater than 1. For the heat fluxes and durations used in this study the numerical model always predicted that no further skin damage was occurring after one minute after the flash fire.

The heat flux at the surface of the mannequin and its variation with time is determined from the recorded temperature data from the sensors. Duhamel's Integral Method is used to convert the measured surface temperature of the sensor into a surface heat flux. The integration is done numerically by the trapezoidal rule. This heat flux is then used as the surface condition in the skin heat transfer model.

The numerical model employs varying thermal physical properties with depth as shown in Table 2. The Crank-Nicolson Implicit method is used with a stretching ratio for the grid spacing in each of the three layers. The grid spacings selected were six in the epidermis, 24 in the dermis and 15 in the subcutaneous. Several different time steps and stretching factors were tested to see which produced the closest result to a base case which could be calculated by hand. The final form uses one second time steps and a stretching ratio of 1.25.

TABLE 2 Parameters Used in Numerical Model of Human Skin

Parameter	Skin Location			
	Epidermis	Dermis	Subcutaneous Tissue	Blood
Overall thickness of layer (m)	8×10^{-5}	2×10^{-3}	1×10^{-2}	...
Thermal conductivity, k (W/m · K)	0.255	0.523	0.167	...
Volumetric heat capacity, $c\rho$ (J/m^3 · K)	4.32×10^6	3.87×10^6	2.76×10^6	3.99×10^6
Blood perfusion rate, G m^3/s/m^3 of tissue	...	1.25×10^{-3}	1.25×10^{-3}	...

As a test of the skin simulant sensor - skin burn - heat transfer model, the calibration lamp was used to heat one of the sensors on the mannequin. The resulting data was loaded into the heat transfer model in order to predict the time required for a second degree burn to occur. Five different heat fluxes were used. These ranged from 5.9 kW/m^2 to 31 kW/m^2 (0.14 cal/cm$^2\cdot$ s to 0.74 cal/cm$^2\cdot$ s). The results are shown in Fig. 6. The time to achieve a second degree burn agrees very well with the experimental results of Stoll and Chianta [9]. This indicates that the mannequin system should give reasonable predictions of the extent and nature of skin burns in the flash fire simulations.

The details of the computer code and the sensor and skin models are given in the Appendix. Included are descriptions of how the numerical code was tested and overall calibration of the sensor-skin-burn model.

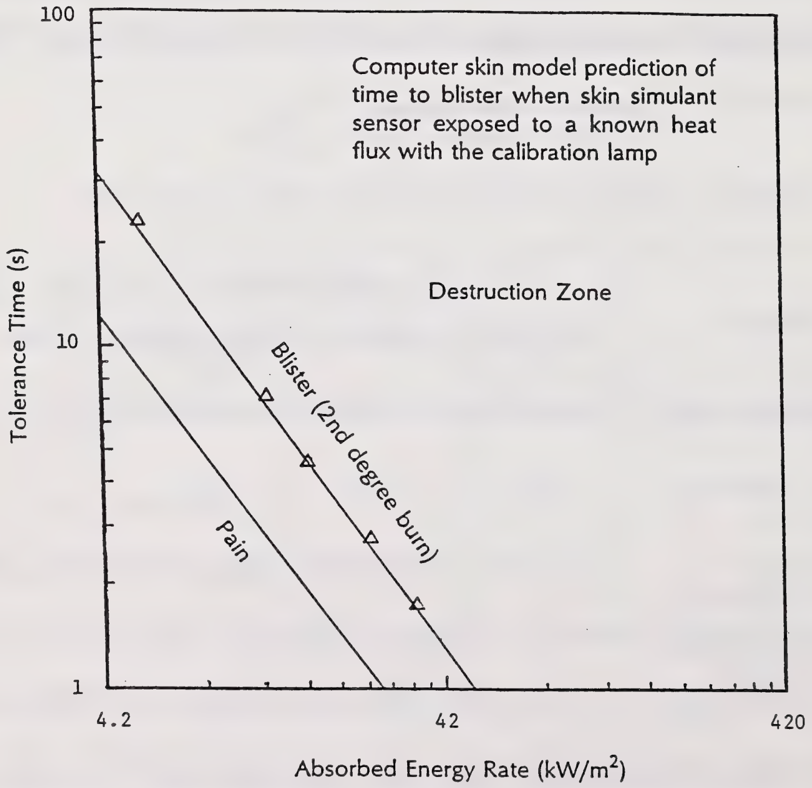

Fig. 6 Human skin tolerance time to absorbed energy showing calibration points obtained using a calibrated heat flux source on a skin simulant sensor

C. GARMENT TESTING WITH VARIED EXPOSURES

Six different protective garment types were exposed to simulated flash fires varying in heat flux and exposure time. Exposures of 67, 75 and 84 kW/m^2 (1.6, 1.8 and 2.0 cal/cm$^2\cdot$s) for three seconds and 67 and 75 kW/m^2 for four seconds were included. Two replications of each test were completed, except that three replications were run for the three seconds, 75 kW/m^2 exposures.

All garments were one-piece coveralls of a similar design. Garments were produced by three different manufacturers and were therefore cut somewhat differently. Garment A was size 42R and fit somewhat snugly on the mannequin. Garment B was size 44 R and fit the mannequin loosely. Garments C, D, E and F were size 42R and fit the mannequin well. All garments were washed once in liquid Tide to remove any residual mill finishes before testing. Laundry conditions included 50°C wash for 10 minutes, cold rinse and either drying in the dryer for 20-30 minutes on the permanent press cycle (for garments D, E and F) or hanging to dry (garments A, B and C).

Characteristics of the garment fabrics, determined using extra fabric samples supplied by the garment manufacturer, are outlined in Table 3 with the standard test procedures noted. Fabric mass was determined prior to laundering; fabric count and thickness were determined after laundering. Thermal protective performance (TPP) was measured after laundering following ASTM D4108, as modified in Par. 6.1 of CAN/CGSB-155.1-M88. This procedure uses an open flame and no spacer between the fabric and the calorimeter. The fabric is held in place in the specimen holder by a set of pins.

TABLE 3 Fabric Characterization and Thermal Protective Performance Ratings of Fabrics Used in Garments Tested

Fibre Content of Garment	Weave	Fabric Count[a] warp/cm × weft/cm	Fabric Mass[b] g/m^2 (oz/yd^2)	Fabric Thickness[c] mm	% Fabric Shrinkage		TPP Value[d] Mean (Std. Dev.)
					warp	weft	
A. Nomex® III (aramid)	Plain	22 × 22	210 (6.2)	0.56	-0.28	1.95	5.2 (± 0.3)
B. 60% Kevlar® (aramid)/ 40% Pbi®	Plain	25 × 20	187 (5.5)	0.54	0.48	0.68	4.3 (± 0.4)
C. Nomex® III (aramid)	Plain (rib variation)	32 × 14	250 (7.4)	0.48	1.19	0.87	4.9 (± 0.3)
D. Proban® FR-7A cotton	Satin	33 × 19	307 (9.1)	0.64	-0.92	4.05	7.2 (± 0.5)
E. Proban® Indura® cotton	Satin	36 × 20	334 (9.9)	0.70	-1.00	0.68	7.3 (± 0.4)
F. Vulkan® (FR viscose/aramid)	Twill	34 × 21	305 (9.0)	0.81	2.32	0.52	6.4 (± 0.2)

[a] CAN/CGSB-4.2 No. 6-M89 (ISO 7211/2-1984), Determination of Number of Threads Per Unit Length, methods A or C.

[b] CAN/CGSB-4.2 No. 5.1-M90, Unit of Mass of Fabrics.

[c] CAN/CGSB-4.2 No. 37-M87, Fabric Thickness, measured at 1.0 kPa (par. 6.3) using small diameter foot.

[d] CAN/CGSB-4.2 No. 58-M90, Method of Colorfastness and Dimensional Change in Domestic Laundering of Textiles (Procedure III).

[e] ASTM D4180-87, Standard Test Method for Thermal Protective Performance of Materials for Clothing by Open-Flame Method, as modified in Par. 6.1 of CAN/CGSB-155.1-M88, Firefighter's Protective Clothing for Protection Against Heat and Flame.

RESULTS

The percent of mannequin surface reaching the 2nd or 3rd-degree burn criteria is reported for each replication of each test in Table 4, demonstrating considerable consistency between replications for any exposure condition. The mean value for each garment type for each heat flux/exposure time combination is given in Fig. 7. All values include 7% for the unprotected head of the mannequin. Since there are no sensors in the hands or feet, however, the maximum possible area reaching the burn criteria is 86%.

Typical computer print-outs of results for garments B and E, exposed at 75 kW/m^2 (1.8 $cal/cm^2 \cdot s$) for both three and four seconds are shown in Figs. 8 to 11. The figures differentiate between the 2nd and 3rd-degree criteria. A typical plot of % burn with time is shown in Fig. 12.

The effect of varying heat flux and exposure time differs with garment type. While the heavier fabrics with the highest TPP values seem to protect very well at the lowest and shortest exposures, the lightest garment with the lowest TPP value (Garment B) gave the best protection from the most severe exposure (4 seconds, 75 kW/m^2). Visual inspection of the garments after exposure indicate that while Garments A, B and C kept their fabric integrity throughout the most severe exposure, Garments D, E and F did not. Garments D and E experienced considerable after flame during this exposure, and when the researchers attempted to remove these garments from the mannequin, they fell apart. The fabric integrity of Garment F was affected less than that of garments D and E. Following exposure, a crystalline material was evident on the inside of Garment F and on the mannequin surface.

These results suggest that the choice of exposure conditions greatly affects the relative results of garment testing on an instrumented mannequin. Thus, whenever possible, exposure conditions should be selected to most closely simulate the hazardous environment from which protection is sought. The results also draw attention to a limitation of the TPP tests in common use. Further investigation of fabric integrity when exposed to high heat flux for exposure over three seconds is recommended.

TABLE 4 Percent of Mannequin Surface Reaching 2nd or 3rd-Degree Burn Criteria[a]

Garment (Rep)	Heat Flux	67 kW/m^2		75 kW/m^2		84 kW/m^2	TPP
	Exp. Time	3 sec	4 sec	3 sec	4 sec	3 sec	Mean (St'd dev.)
A (1)		15.3	46.8	29.0	63.3	45.2	5.2
(2)		16.8	56.6	37.4	66.1	35.8	(±0.3)
(3)				33.6			
B (1)		10.4	30.5	12.3	47.3	17.5	4.3
(2)		10.4	24.7	13.1	47.5	13.9	(±0.4)
(3)				11.7			
C (1)		8.4	28.7	17.5	55.1	28.7	4.9
(2)		8.3	30.4	11.7	51.9	26.6	(±0.3)
(3)				18.2			
D (1)		8.5	34.5	9.8	70.8	10.2	7.3
(2)		7.9	26.4	11.3	75.5	10.3	(±0.5)
(3)				9.9			
E (1)		8.5	37.6	9.8	80.4	13.3	7.3
(2)		8.8	24.4	10.7	81.5	9.7	(±0.4)
(3)				8.8		9.1	
F (1)		14.4	32.1	14.7	58.3	15.7	6.4
(2)		11.6	32.7	17.3	65.7	13.9	(±0.2)
(3)				13.4			

[a] Maximum possible % is 86, since hands and feet do not have sensors; figures include 7% unprotected mannequin in the head area:

Garments A: 210 g (6.2 oz) plain weave Nomex® III (aramid), size 42R (close-fitting)
B: 187 g (5.5 oz) plain weave 60/40 Kevlar® (aramid)/Pbi®, size 44
C: 249 g (7.4 oz) rib weave Nomex® III (aramid), size 42R
D: 307 g (9.1 oz) satin weave Proban® FR-7A cotton, size 42R
E: 334 g (9.9 oz) satin weave Indura® Proban® cotton, size 42R
F: 305 g (9.0 oz) twill weave Vulkan® (FR viscose/aramid), size 42R

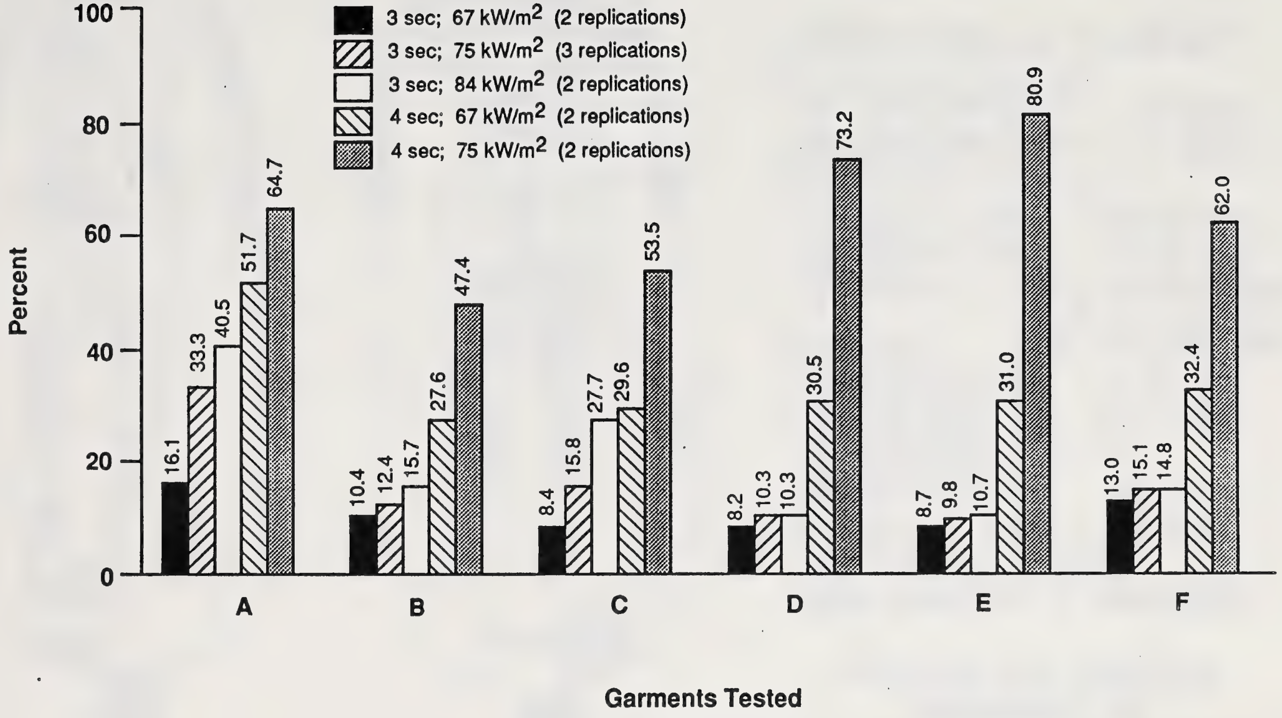

Fig. 7 Mean percent mannequin surface reaching 2nd or 3rd degree burn criteria
(Note: Maximum possible % is 86, as hands and feet do not have sensors; all figures include 7% unprotected mannequin in the head area.)

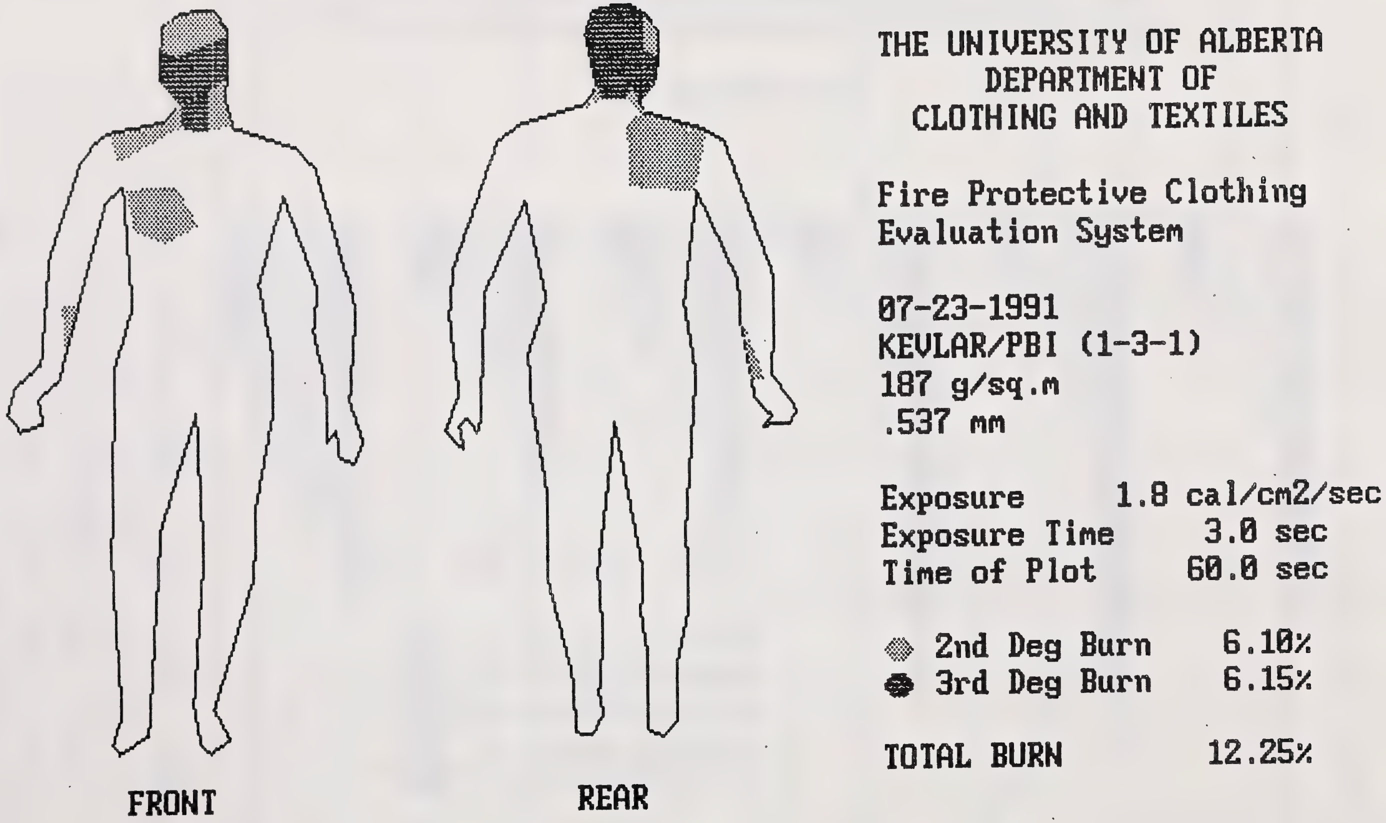

```
THE UNIVERSITY OF ALBERTA
      DEPARTMENT OF
  CLOTHING AND TEXTILES

Fire Protective Clothing
Evaluation System

07-23-1991
KEVLAR/PBI (1-3-1)
187 g/sq.m
.537 mm

Exposure      1.8 cal/cm2/sec
Exposure Time      3.0 sec
Time of Plot      60.0 sec

▨ 2nd Deg Burn     6.10%
● 3rd Deg Burn     6.15%

TOTAL BURN        12.25%
```

Fig. 8 Calculated location of skin burning on mannequin
Garment B, 75 kW/m^2, 3 second exposure

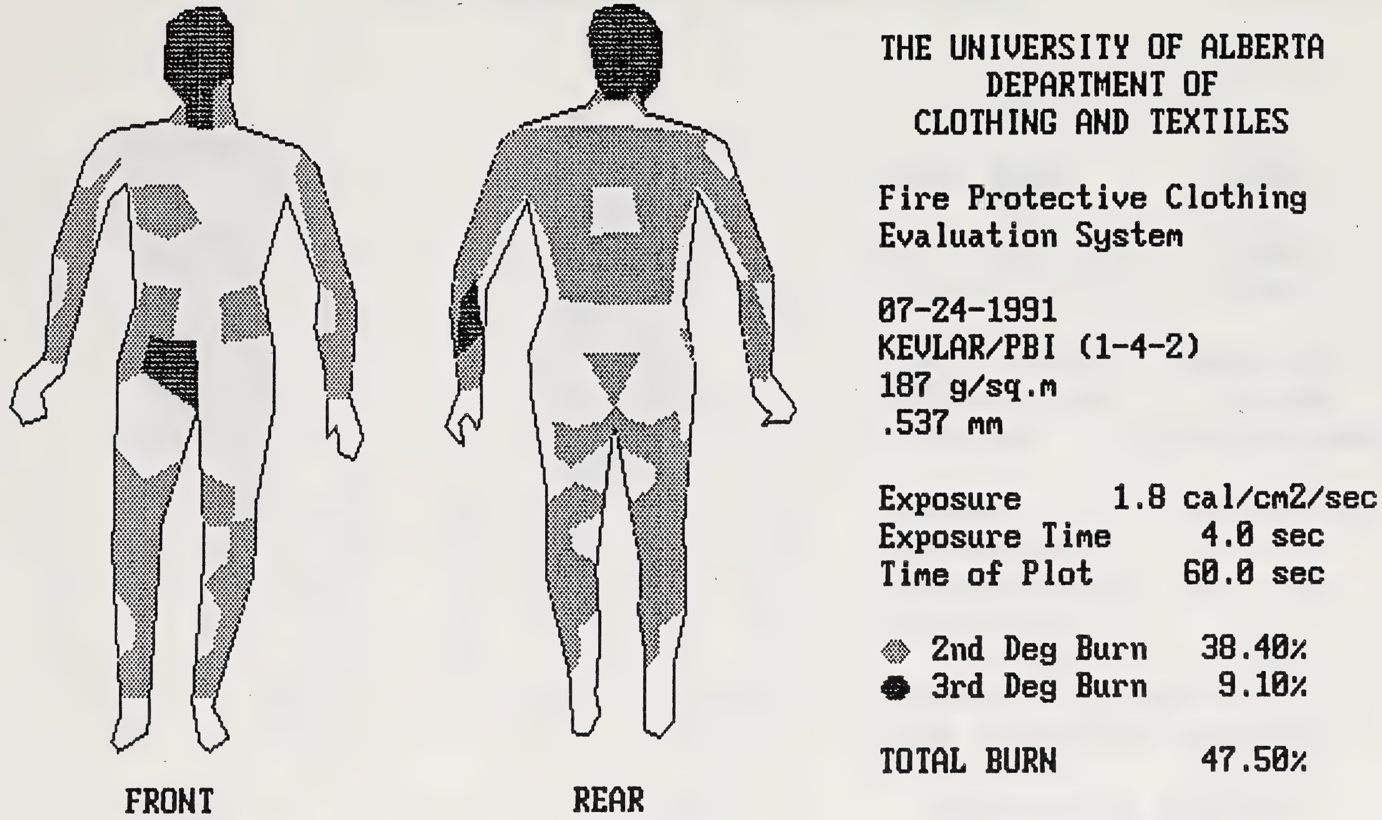

```
THE UNIVERSITY OF ALBERTA
   DEPARTMENT OF
 CLOTHING AND TEXTILES

Fire Protective Clothing
Evaluation System

07-24-1991
KEVLAR/PBI (1-4-2)
187 g/sq.m
.537 mm

Exposure      1.8 cal/cm2/sec
Exposure Time      4.0 sec
Time of Plot      60.0 sec

▨ 2nd Deg Burn   38.40%
● 3rd Deg Burn    9.10%

TOTAL BURN       47.50%
```

Fig. 9 Calculated location of skin burning on mannequin
Garment B, 75 kW/m^2, 4 second exposure

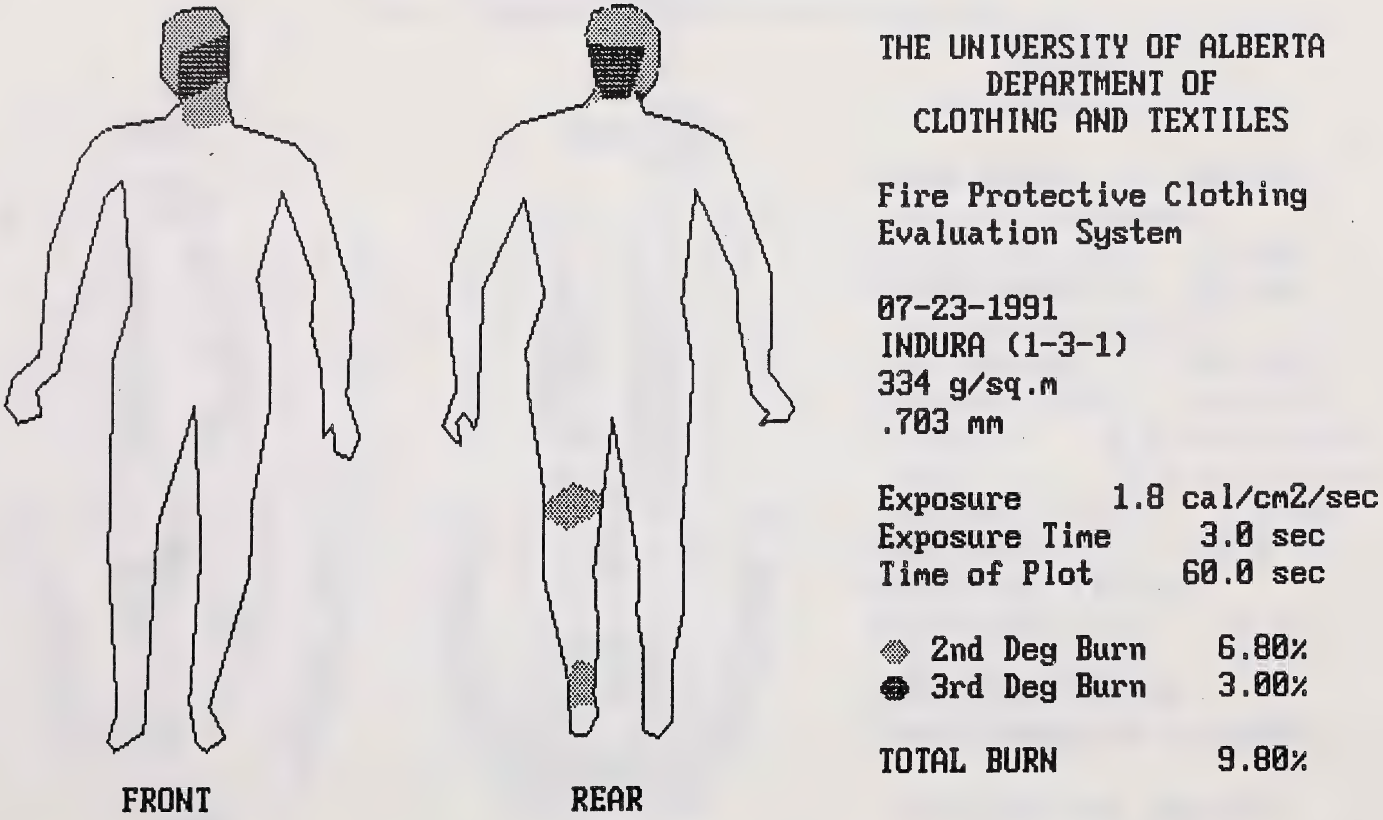

```
THE UNIVERSITY OF ALBERTA
      DEPARTMENT OF
 CLOTHING AND TEXTILES

Fire Protective Clothing
Evaluation System

07-23-1991
INDURA (1-3-1)
334 g/sq.m
.703 mm

Exposure      1.8 cal/cm2/sec
Exposure Time     3.0 sec
Time of Plot     60.0 sec

◈ 2nd Deg Burn     6.80%
● 3rd Deg Burn     3.00%

TOTAL BURN         9.80%
```

Fig. 10 Calculated location of skin burning on mannequin
Garment E, 75 kW/m^2, 3 second exposure

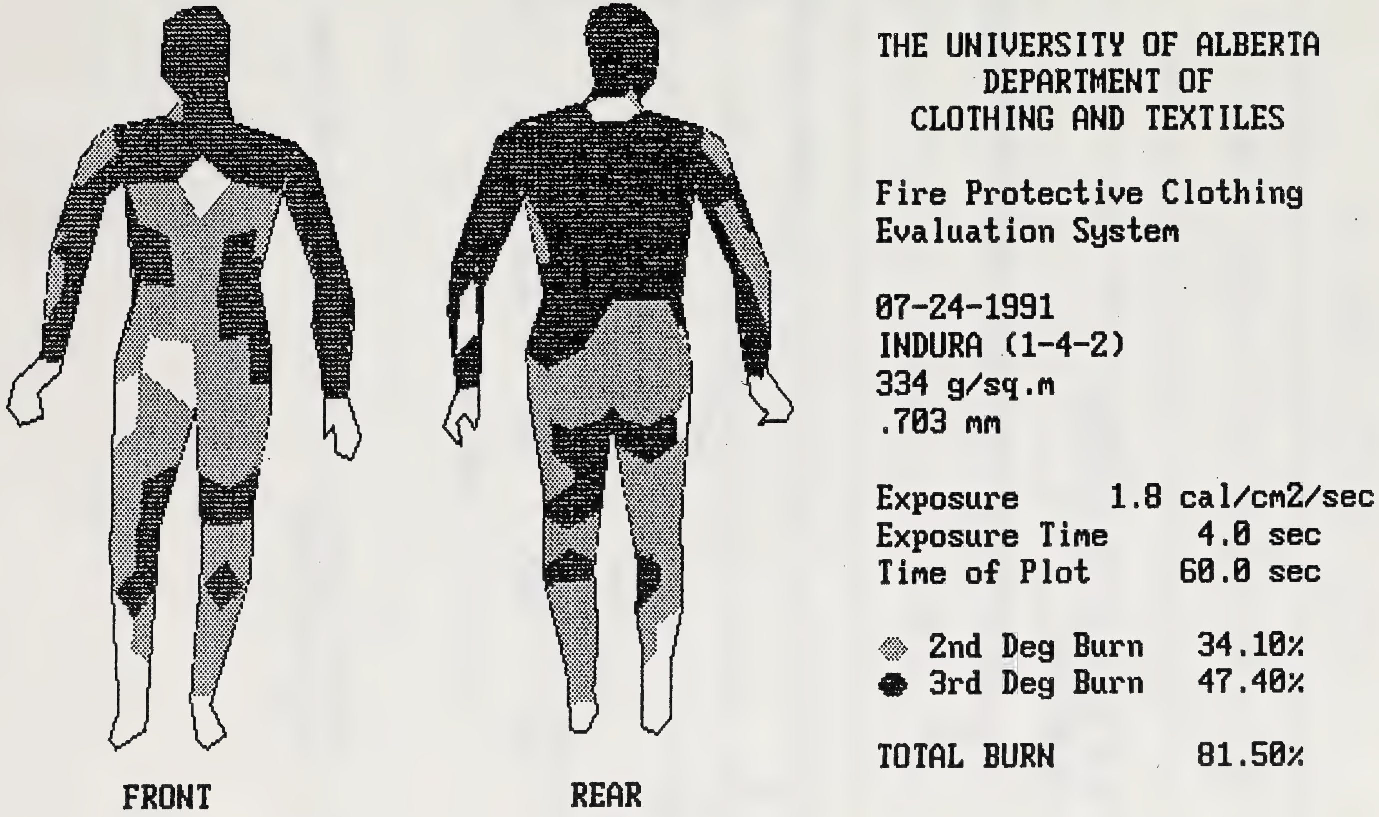

```
THE UNIVERSITY OF ALBERTA
     DEPARTMENT OF
  CLOTHING AND TEXTILES

Fire Protective Clothing
Evaluation System

07-24-1991
INDURA (1-4-2)
334 g/sq.m
.703 mm

Exposure      1.8 cal/cm2/sec
Exposure Time      4.0 sec
Time of Plot      60.0 sec

▨ 2nd Deg Burn    34.10%
● 3rd Deg Burn    47.40%

TOTAL BURN        81.50%
```

Fig. 11 Calculated location of skin burning on mannequin
Garment E, 75 kW/m^2, 4 second exposure

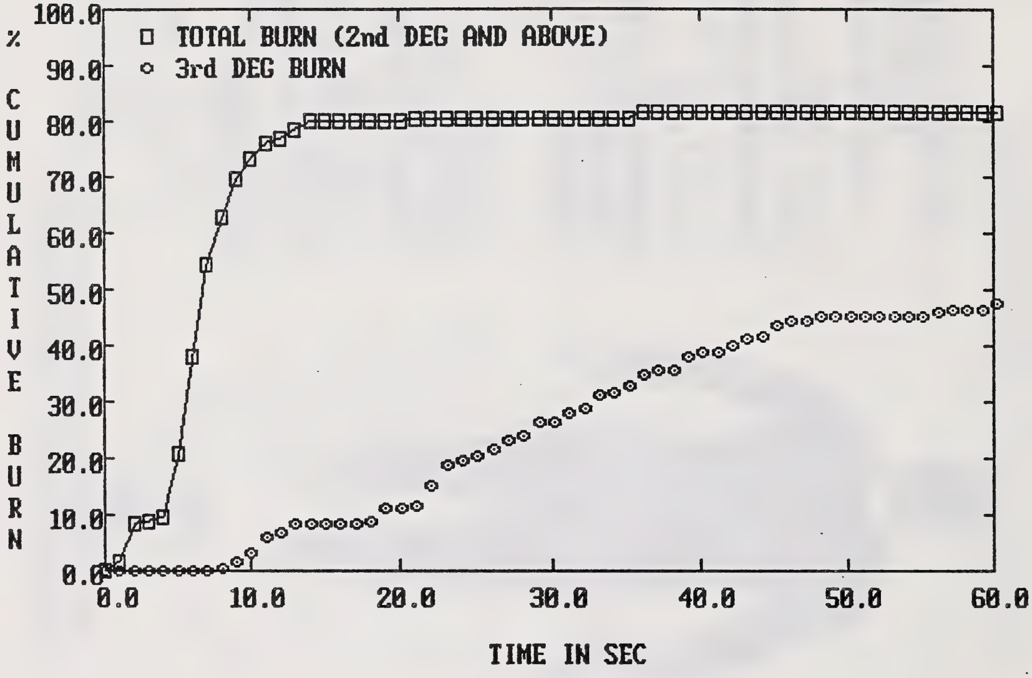

Fig. 12 Calculated cumulative skin burning for a typical 4 second exposure with protective clothing

D. SUMMARY AND CONCLUSIONS

A full-sized instrumented mannequin has been developed which can be used to evaluate the thermal protective qualities of garments in flash fires or fire balls of varying intensity and duration. Garment testing has shown that, in general, increasing the fabric weight and/or thickness for a particular fiber or fiber/finish combination reduces the extent of skin burning. However, fabrics of some polymeric materials (e.g. Pbi®) offer more protection than others, so that a general correlation between thickness/weight and protection does not hold, especially at higher heat fluxes and durations. TPP values correlate better with the predicted amount of skin burning on the mannequin at low heat flux/duration than at higher heat flux/duration exposures.

The results of this research indicate that for garment testing, exposure conditions should be selected to simulate actual flash fire/fireball hazards. The effect of fabric integrity on protection at high exposures (both heat flux and duration) needs further investigation.

REFERENCES

[1] Crown, E.M., Rigakis, K.B. and Dale, J.D., "Systematic Assessment of Protective Clothing for Alberta Workers", final research report prepared for Alberta Occupational Health and Safety, Edmonton, Alberta, June 15, 1989, pp. 1-487.

[2] Buettner, K., "Effects of Extreme Heat and Cold on Human Skin. I. Analysis of Temperature Changes Caused by Different Kinds of Heat Application", Journal of Applied Physiology, Vol. 3, p. 691, 1951.

[3] Mehta, A.K. and Wong, F., "Measurement of Flammability and Burn Potential of Fabrics", Fuels Research Laboratory, M.I.T. Summary Report DSR 73884, Feb. 15, 1973.

[4] Elkins, W. and Thompson, J.G., "Instrumentated Thermal Mannikin", Aerotherm Division/Acurex Corporation, Final Report AD-781176, January, 1973.

[5] Henriques, F.C. and Moritz, A.R., "Studies of Thermal Injury: I. The Conduction of Heat to and Through Skin and the Temperatures Attained Therein. A Theoretical and an Experimental Investigation", American Journal of Pathology, Vol. 23, p. 531, 1947.

[6] Henriques, F.C., "Studies of Thermal Injury: V. The Predictability and the Significance of Thermally Induced Rate Processes Leading to Irreversible Epidermal Injury", Archives of Pathology, Vol. 43, p. 489, 1947.

[7] Morse, H., Tickner, G. and Brown, R., "Burn Damage and Burn Depth Criteria", Aerotherm Report TN-75-26, Jan. 1975.

[8] Stoll, A.M. and Greene, L.C., "Relationship Between Pain and Tissue Damage Due to Thermal Radiation", Journal of Applied Physiology, Vol. 14, p. 373, 1959.

[9] Stoll, A.M. and Chianta, M.A., "Method and Rating System for Evaluation of Thermal Protection", Aerospace Medicine, Vol. 40, p. 1232, 1969.

[10] Takata, A.N., Rouse, J. and Stanley, T., "Thermal Analysis Program", I.I.T. Research Institute Report, IITRI-J6286, Feb. 1973.

APPENDIX

A COMPUTER CODE FOR ESTIMATING THERMAL INJURY OF HUMAN SKIN

This program was written in QuickBasic 4.5™ for using data from an instrumented mannequin to estimate the nature and amount of skin burning when the mannequin is exposed to flash fires. In general, the program uses Duhamel's Integral Method to calculate the surface heat flux from the measured surface temperatures of the sensors. On the basis of the calculated surface heat flux, a multi-layer skin model is solved for the skin temperatures using the Crank-Nicolson Implicit method. From the skin temperature distribution, the degree of thermal injury and the depth of damage for each location of the body are determined by a first order reaction rate process equation coupled with a burn criterion from the literature. The percentage of the total area burned is then estimated based on the number of sensors which indicate 2nd degree burn or above. The program also draws the burned area of the mannequin at each second of realtime up to any chosen time period (max. 2 minutes) and plots the percent cumulative burn versus time. In this program integrations of all time functions are performed using the trapezoidal rule and the thermal response of the skin is assumed to be independent of site. The above procedures are described in Fig. A1.

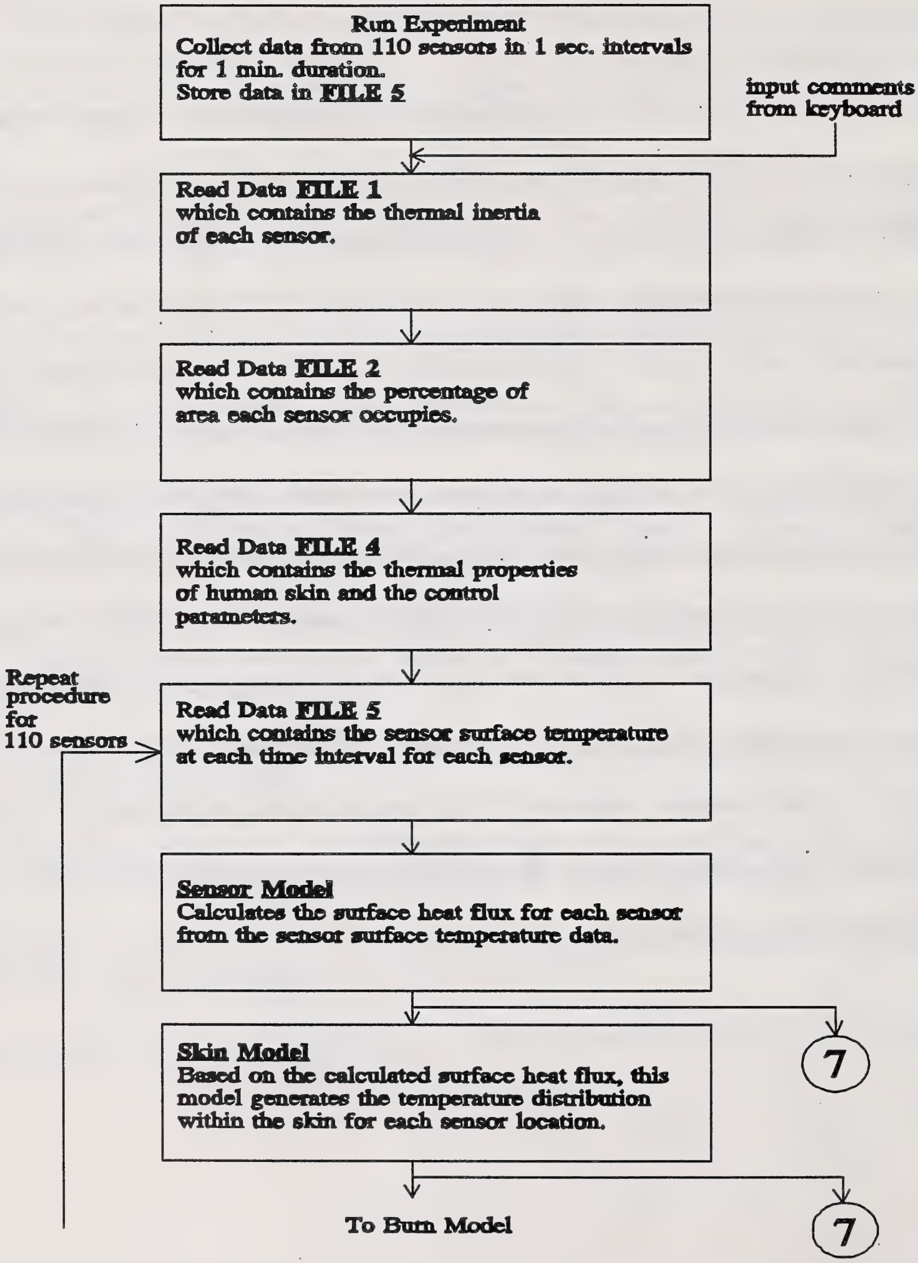
Run Experiment
Collect data from 110 sensors in 1 sec. intervals for 1 min. duration.
Store data in FILE 5
input comments from keyboard
Read Data FILE 1
which contains the thermal inertia of each sensor.
Read Data FILE 2
which contains the percentage of area each sensor occupies.
Read Data FILE 4
which contains the thermal properties of human skin and the control parameters.
Repeat procedure for 110 sensors
Read Data FILE 5
which contains the sensor surface temperature at each time interval for each sensor.
Sensor Model
Calculates the surface heat flux for each sensor from the sensor surface temperature data.
7
Skin Model
Based on the calculated surface heat flux, this model generates the temperature distribution within the skin for each sensor location.
To Burn Model
7

Fig. A1 The Flow Diagram of the Program

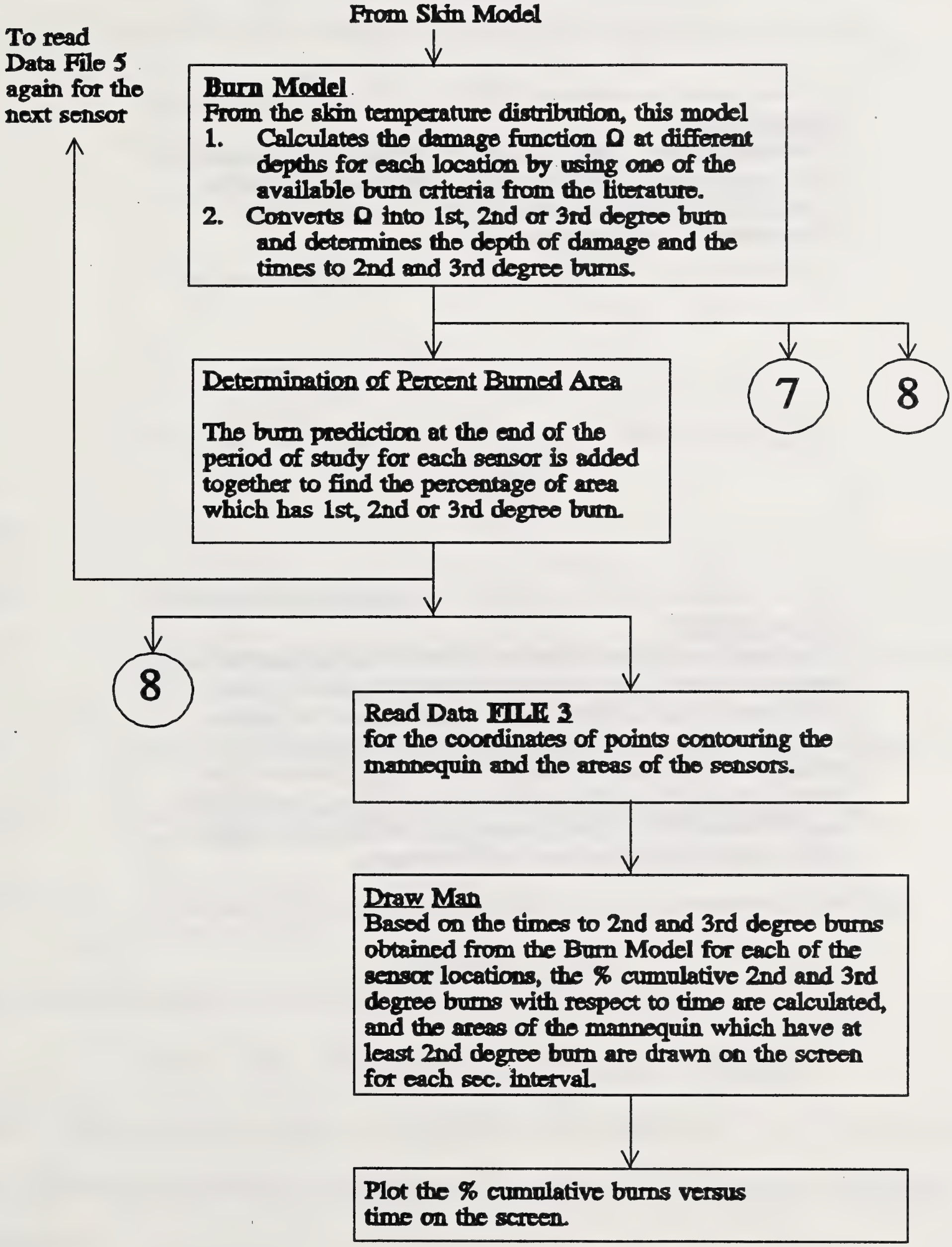

Burn Model
From the skin temperature distribution, this model

1. Calculates the damage function Ω at different depths for each location by using one of the available burn criteria from the literature.
2. Converts Ω into 1st, 2nd or 3rd degree burn and determines the depth of damage and the times to 2nd and 3rd degree burns.

Determination of Percent Burned Area

The burn prediction at the end of the period of study for each sensor is added together to find the percentage of area which has 1st, 2nd or 3rd degree burn.

Read Data **FILE 3**
for the coordinates of points contouring the mannequin and the areas of the sensors.

Draw Man
Based on the times to 2nd and 3rd degree burns obtained from the Burn Model for each of the sensor locations, the % cumulative 2nd and 3rd degree burns with respect to time are calculated, and the areas of the mannequin which have at least 2nd degree burn are drawn on the screen for each sec. interval.

Plot the % cumulative burns versus time on the screen.

Fig. A1 (continued)

⑦

Output FILE 7
Contains the time - heat flux - sensor surface temperature - skin temperature distribution data, and the damage function Ω at the basal layer and at the depth of damage for any chosen sensor locations (optional).

⑧

Output FILE 8
Contains the summary of sensor response and the mannequin burn prediction. The former includes the times to 2nd and 3rd degree burns, the total accumulated heats at 2nd degree burn and at the end of the period of study, the depth of damage and the predicted degree burn for each sensor. The latter includes the predicted percent areas of 1st, 2nd and 3rd degree burns for the whole mannequin, and the sums of the total accumulated heats for all of the sensors.

Fig. A1 (continued)

The input data required for this program are stored in 5 data files. File 1 contains mainly the thermal inertia (kρC) of the sensors. The data in File 1 are formatted as follows:

NSEN			
NOS_1	KPC_1	$SLOPE_1$	$INTERCEPT_1$
NOS_2	KPC_2	$SLOPE_2$	$INTERCEPT_2$
.	.	.	.
.	.	.	.
.	.	.	.
.	.	.	.
$NOS_{(NSEN)}$	$KPC_{(NSEN)}$	$SLOPE_{(NSEN)}$	$INTERCEPT_{(NSEN)}$

Where:

NSEN = Total number of sensors

NOS_i = A sensor number which identifies the location of the sensor on the mannequin. The subscript i indicates the i-th sensor on the file.

KPC_i = The thermal inertia of the sensor identified by NOS_i, cal^2/cm^4·°C^2·sec.

$SLOPE_i$ = The slope of the calibration line for the sensor identified by NOS_i, cm^2·°C·sec$^{0.5}$/cal.

$INTERCEPT_i$ = The intercept of the calibration line for the sensor identified by NOS_i, °C·cm^2·sec/cal.

File 2 contains the percent area each sensor occupies (PCT) which are formatted as:

$$NOS_1 \quad PCT_1 \quad NOS_2 \quad PCT_2 \, ... \, NOS_{(NSEN)} \quad PCT_{(NSEN)}$$

File 3 is required only for drawing the mannequin and its burned area. Thus File 3 consists of the coordinates which contour the mannequin and the areas of the sensors. These data are formatted as:

N1			
FX_1	FX_2	....	$FX_{(N1)}$
FY_1	FY_2	....	$FY_{(N1)}$
N2			
BX_1	BX_2	.....	$BX_{(N2)}$
BY_1	BY_2	....	$BY_{(N2)}$
N3			
$FXMAN_1$	$FXMAN_2$	....	$FXMAN_{(N3)}$
$FYMAN_1$	$FYMAN_2$	....	$FXMAN_{(N3)}$
N4			
$BXMAN_1$	$BXMAN_2$	....	$BXMAN_{(N4)}$
$BYMAN_1$	$BYMAN_2$	....	$BYMAN_{(N4)}$

Where:

N1 = No. of points required to outline the front view of the mannequin

FX_i = X-coordinate for the front view of the outline of the mannequin

FY_i = Y-coordinate for the front view of the outline of the mannequin

N2 = No. of points required to outline the back view of the mannequin

BX_i = X-coordinate for the back view of the outline of the mannequin

BY_i = Y-coordinate for the back view of the outline of the mannequin

N3 = No. of points required to outline the front view of the areas of the sensors

$FXMAN_i$ = X-coordinate for the front view of the areas of the sensors

$FYMAN_i$ = Y-coordinate for the front view of the areas of the sensors

N4 = No. of points required to outline the back view of the areas of the sensors

$BXMAN_i$ = X-coordinate for the back view of the areas of the sensors

$BYMAN_i$ = Y-coordinate for the back view of the areas of the sensor

and, subscript i = the i-th coordinate point.

In File 4, all the thermal properties of human skin and the control parameters are included. The format of the data in this file is shown as follows:

```
 Mode 1      Mode 2      DT        NST
NG1         NG2   NG3   NS1        NS2   NS3
R1          R2    R3
TI          TB    CPB   H
THK(1)      THK(2)      THK(3)
CP(1)       CP(2)       CP(3)
COND(1)     COND(2)     COND(3)
G(1)        G(2)        G(3)
GAMA(1)     GAMA(2)
```

Where:

Mode 1 = A mode number for selecting the type of skin
  1. for opaque skin (ignore penetrating radiant heat)
  2. for diathermanous skin (include penetrating radiant heat)

Mode 2 = A mode number for selecting the burn criteria
  1. for Henriques' criteria
  2. for Stoll's criteria
  3. For M.I.T.'s criteria
  4. combined criteria of Stoll's for epidermal burn and Takata's for dermal layer

DT = time step, sec.

NST = printing steps for time

NG1 = No. of grid in epidermis

NG2 = No. of grid in dermis

NG3 = No. of grid in subcutaneous tissue

NS1 = printing steps for NG1

NS2 = printing steps for NG2

NS3 = printing steps for NG3

R1 = axial stretching ratio for epidermis

R2 = axial stretching ratio for dermis

R3 = axial stretching ratio for subcutaneous tissue

TI = initial temperature at skin surface, °C

TB = blood temperature, °C

CPB = volumetric heat capacity of blood, $cal/cm^3 \cdot °C$

H = overall surface heat loss coefficient, $cal/cm^2 \cdot sec \cdot °C$

THK(k) = thickness of the k-th layer of skin, cm

Cp(k) = volumetric heat capacity of the k-th layer of skin, $cal/cm^3 \cdot °C$

COND(k) = conductivity of the k-th layer of skin, $cal/cm \cdot °C \cdot sec$

G(k) = blood perfusion rate for skin layer k, cm^3/sec per cm^3 of tissue

GAMA(1) =absorption coefficient of epidermis, cm^{-1}

GAMA(2) =absorption coefficient of dermis and subcutaneous tissue, cm^{-1}

and, k = 1 for epidermis
= 2 for dermis
= 3 for subcutaneous tissue

The last data file, File 5, stores all the measured surface temperatures of the sensors at each time interval in the following format:

```
NOS(1)
      TSS(1)   TSS(2)   ...   999.9
NOS(2)
      TSS(1)   TSS(2)   ...   999.9
.
.
.
NOS(NSEN)
      TSS(1)   TSS(2)   ...   999.9
```

Where:

NOS(M) = The sensor number of the M-th sensor the file stores its temperatures

TSS(J) = The measured sensor surface temperature at the J-th point in time, °C

The number 999.9 at the end of each temperature line is used to indicate the end of the data for one sensor.

In addition to the input data stored in the files as mentioned previously, the program also requires some other information. This information is input directly from the keyboard and include the following:

COVER = Type of clothing system

WEIGHT = Fabric mass, g/m^2

FABTHK = Fabric thickness, mm

XPS = Exposure heat flux, $cal/cm^2 \cdot sec$

XPSTME = Exposure time, sec

NSENP = Number of sensors selected for printing

NOSP = Selected sensor numbers for printing

TA = Ambient temperature, °C

TMC = Calculation time, sec

In the following sections, the sensor model, the skin model and the burn model will be discussed in detail.

SENSOR MODEL

This model assumes that the sensor (the skin simulant) is a semi-infinite solid with constant thermal properties and the heat transfer phenomena obey the one-dimensional Fourier equation:

$$\frac{\partial T}{\partial t} = \alpha \frac{\partial^2 T}{\partial x^2} \qquad \text{(A1)}$$

where T =temperature, °C

t =time, sec

x =distance below the surface, cm

α = k/ρC = thermal diffusivity, cm^2/sec

k =thermal conductivity, cal/cm·sec·°C

ρ = density, g/cm^3

C = specific heat capacity, cal/g·°C

These are valid assumptions for the short time periods involved with flash fires.

Given the measured surface temperature, this model calculates the surface heat flux of the sensor using the Duhamel's Integral Method.

The Duhamel's theorem states that if $u_1(x,t)$ is the response of a linear homogeneous system (initially at zero) to a single unit step input, the response $u_F(x,t)$ of the system to the input F(t) is given by the following equation:

$$u_F(x,t) = \int_o^t F(\tau) \frac{\partial u_1(x,t-\tau)}{\partial t} d\tau \qquad \text{(A2)}$$

In order to calculate the surface heat flux based on the measured surface temperature using the Duhamel's theorem, one has to know how the surface heat flux responds to a single unit step increase in surface temperature. The classical solution of Eq. (A1) for the temperature response of a semi-infinite solid initially at T_i and subjected to a step change in surface temperature T_s at zero time has been given in the literature [A6]:

$$\frac{T-T_i}{T_s-T_i} = 1-\frac{2}{\sqrt{\pi}}\int_o^{x/2\sqrt{\alpha t}} e^{-y^2}dy \tag{A3}$$

Thus the surface heat flux q is:

$$\begin{aligned} q(t) &= -k\,\frac{\partial T}{\partial x}\Big|_{x=0} = \frac{2k}{\sqrt{\pi}}\,(T_s-T_i)\,\frac{\partial}{\partial x}\int_o^{x/2\sqrt{\alpha t}} e^{-y^2}dy \\ &= \frac{2k}{\sqrt{\pi}}\,(T_s-T_i)\left[\frac{\partial}{\partial(x/2\sqrt{\alpha t})}\int_o^{x/2\sqrt{\alpha t}} e^{-y^2}dy\right]\frac{\partial(x/2\sqrt{\alpha t})}{\partial x} \\ &= \frac{2k}{\sqrt{\pi}}\,(T_s-T_i)\left\{e^{-x^2/4\alpha t}\,\frac{1}{2\sqrt{\alpha t}}\right\}_{x=0} \\ &= \frac{k}{\sqrt{\pi\alpha t}}\,(T_s-T_i) \end{aligned} \tag{A4}$$

For a single unit step increase in surface temperature, T_s - T_i = 1. Thus, the heat flux response (initially at zero) becomes:

$$q(t) = \frac{k}{\sqrt{\pi\alpha t}} \tag{A5}$$

Substituting Eq. (A5) into Eq. (A2), the corresponding heat flux for a variable surface temperature is:

$$Q(t) = \int_o^t (T_s(\tau) - T_i) \frac{\partial q(t-\tau)}{\partial t} d\tau$$

$$= \frac{k}{2\sqrt{\pi\alpha}} \left[\int_o^t \frac{T_s(t) - T_s(\tau)}{(t-\tau)^{3/2}} d\tau + \int_o^t \frac{T_i - T_s(t)}{(t-\tau)^{3/2}} d\tau \right]$$

$$Q(t) = \sqrt{\frac{k\rho C}{\pi}} \left[\frac{1}{2} \int_o^t \frac{T_s(t) - T_s(\tau)}{(t-\tau)^{3/2}} d\tau + \frac{T_s(t) - T_i}{t^{(1/2)}} \right] \qquad \text{(A6)}$$

The integral in Eq. (A6) can be evaluated easily by standard numerical integration methods such as the trapezoidal rule.

One criterion for choosing the skin simulant is that its thermal inertia, kρC, should match that of the skin [A3]. To find the thermal inertia, the surface of the simulant was irradiated with a known constant heat flux, and the surface temperature rise (ΔT) with time was measured. The thermal inertia can then be obtained from Eq. (A7), given in Reference [A6], describing the temperature response of a semi-infinite solid initially at T_i to a constant heat flux q at t = 0:

$$T(x,t) - T_i = \frac{q}{k} \left[2\sqrt{\frac{\alpha t}{\pi}}\, e^{-\frac{x^2}{4\alpha t}} - x \, erfc\left(\frac{x}{2\sqrt{\alpha t}} \right) \right] \qquad \text{(A7)}$$

At x = 0, Eq. (A7) becomes:

$$\frac{\Delta T}{q} = \frac{2}{\sqrt{k\rho C\pi}} \sqrt{t} \qquad \text{(A8)}$$

Thus, by plotting ΔT/q vs. √t, kρC can be calculated from the slope 2/√kρCπ.

The skin simulant is an inorganic mixture of calcium, aluminum, silicate with asbestos fibres and a binder, which is called "Colorceran". Each sensor which is made up of this material, is about 19 mm in diameter and 32 mm long. To measure the surface temperature a 30 gauge

Cu-Co thermal couple wire rolled flat to about 0.1 mm thick was held on the surface with an epoxy-phenolic adhesive. Figure A2 shows the plot of Eq. (A8) for a test sensor. The thermal inertia calculated from the slope is about 12.53 × 10^{-4} $cal^2/cm^4 \cdot °C^2 \cdot sec$. The density of this material was measured to be 1.877 g/cm^3. The heat conductivity obtained from an independent measurement [A7] was approximately 0.97 W/mK (23.18 × 10^{-4} cal/cm·sec·°C). Once these thermal properties are known, the specific heat capacity and diffusivity can easily be calculated. These are summarized in Table A1 in which the thermal properties of human skin [3,8] are also included.

TABLE A1 Thermal Properties of Human Skin and Skin Simulant

Properties	Human Skin		Skin Simulant
	Epidermis	Dermis	
k(cal/cm·sec·°C)	6.1×10^{-4}	12.5×10^{-4}	23.18×10^{-4}
ρ(g/cm^3)	1.2	1.2	1.877
C(cal/g·°C)	0.86	0.77	0.288
α(cm^2/sec)	5.91×10^{-4}	13.53×10^{-4}	42.88×10^{-4}
$k\rho C$($cal^2/cm^4 \cdot °C^2 \cdot sec$)	6.30×10^{-4}	11.55×10^{-4}	12.53×10^{-4}

As seen in Table A1, the thermal inertia of the skin simulant is within 10% of that of the dermis which occupies about 96% of the thickness of the skin. Therefore, "Colorceran" is appropriate for using as a skin simulant.

There were 110 of these skin simulant sensors installed on the mannequin. Each of these sensors was calibrated using the same method. The variation of the thermal inertia for these sensors are shown in Fig. A3. As indicated, the mean thermal inertia is 11.71 × 10^{-4} $cal^2/cm^4 \cdot °C^2 \cdot sec$ with a standard deviation of 1.11 × 10^{-4}.

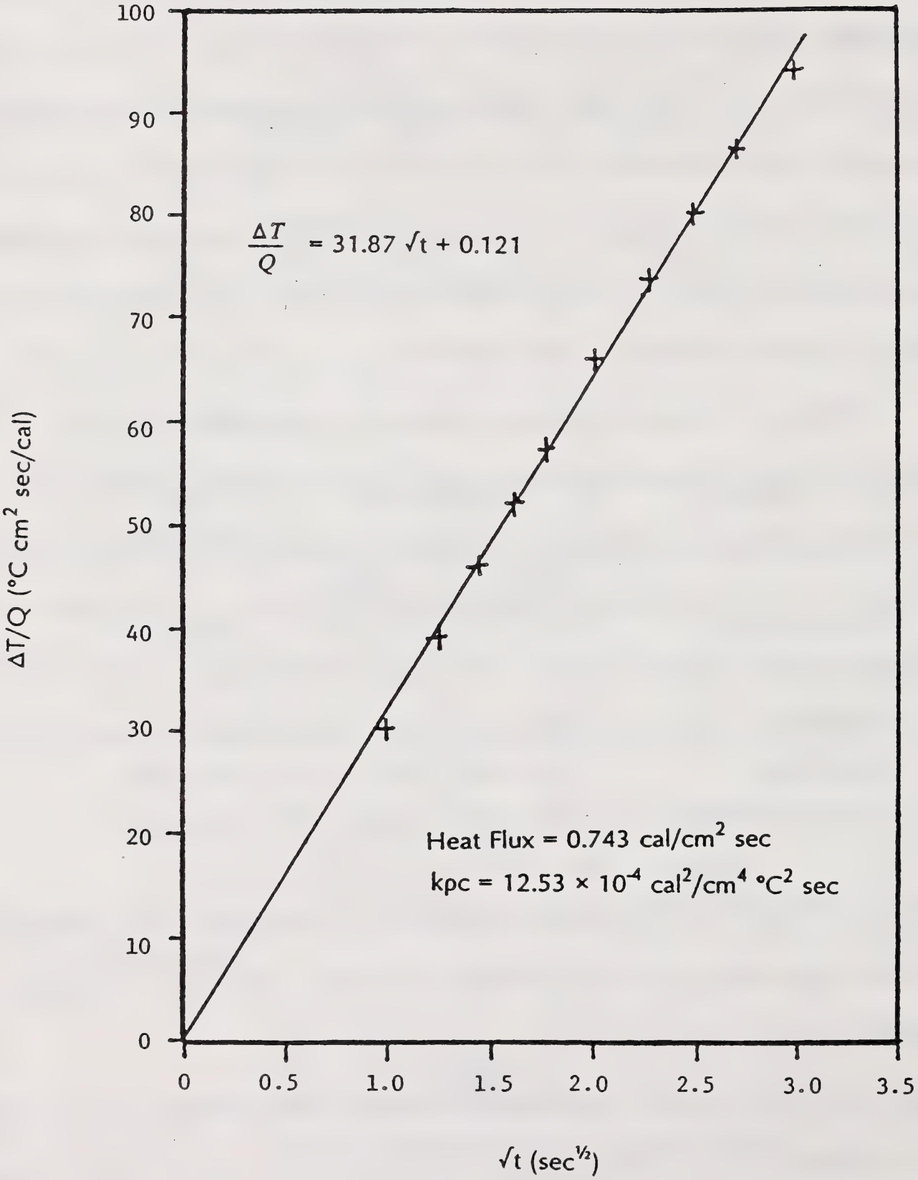

Fig. A2 Calibration result of the thermal inertia of a skin simulant sensor

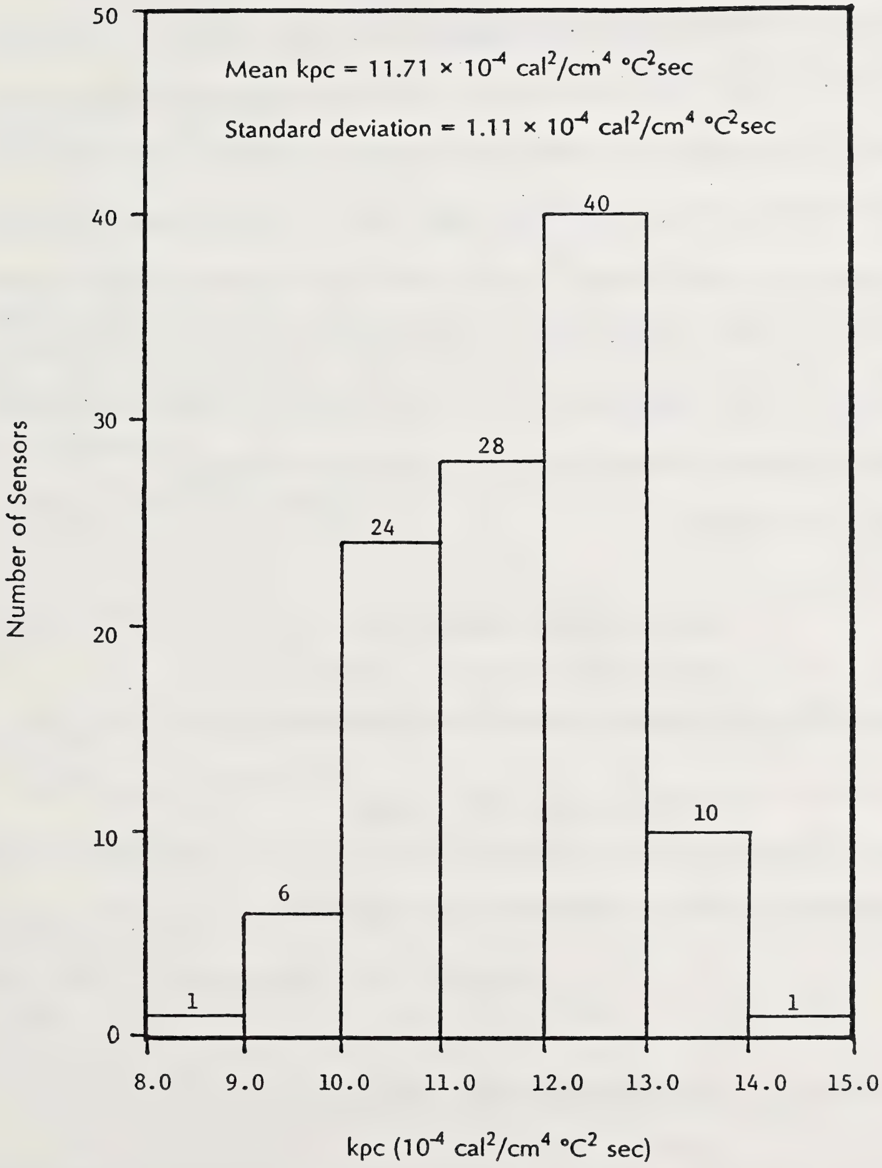

Fig. A3 Variation of the thermal inertia of the 110 skin simulants

Due to the surface condition of the sensors and the adhesion situation between the thermal couples and the surfaces, the plots of Eq. (A8) usually do not intercept exactly at the origin. The mean Y-intercept of the 110 sensors was found to be -1.5326 °C·cm^2·sec/cal with a standard deviation of 1.989. The negative value of the mean Y-intercept indicates a time lag in initial response for the majority of the sensors and the time lag is equal to (Y-intercept/slope)^2.

Since the Duhamel's Integral Method is only applicable to a linear homogeneous system of which the response to an input function is initially at zero (i.e. for Y-intercept equal zero), the calculation of the heat flux using this method by neglecting the Y-intercept would lead to a computational error. Thus a simple method was derived to correct the prediction of heat flux using the Duhamel's Integral Method without consideration of the Y-intercept.

Recall Eq. (A8). That is:

$$\frac{\Delta T}{q} = slope\ \sqrt{t} \qquad \text{(A8)}$$

where slope = $2/\sqrt{k\rho C\pi}$. With intercept included, Eq. (A8) becomes:

$$\frac{\Delta T}{q} = slope\ \sqrt{t} + intercept$$

To predict the heat flux (q_1) without consideration of the intercept:

$$q_1(t) = \frac{\Delta T}{slope\ \sqrt{t}} \qquad \text{(A8a)}$$

To predict the heat flux (q_2) with consideration of the intercept:

$$q_2(t) = \frac{\Delta T}{slope\ \sqrt{t} + intercept} \qquad \text{(A8b)}$$

To predict q_2 from q_1, combine Eqs. (A8a) and (A8b):

$$\frac{q_2(t)}{q_1(t)} = \frac{slope\sqrt{t}}{slope\sqrt{t} + intercept} = \frac{1}{1 + \frac{intercept}{slope}\frac{1}{\sqrt{t}}}$$

so that $q_2(t) = CF \times q_1(t)$ where

$$CF = \frac{1}{1 + \frac{intercept}{slope}\frac{1}{\sqrt{t}}} \tag{A9}$$

As indicated in Eq. (A9), when time increases, CF increases if the intercept is positive, or decreases if the intercept is negative. When time tends to infinity, CF tends to one. Equation (A9) also indicates that:

When $t > 100\ (intercept/slope)^2$,

$$CF \begin{cases} > 0.91 \quad and \quad \leq 1 \quad for\ positive\ intercept \\ \geq 1 \quad and \quad < 1.11 \quad for\ negative\ intercept \end{cases}$$

For the test results shown in Fig. A3, the mean slope and intercept are about 33.0 $cm^2 \cdot {}^\circ C \cdot sec^{1/2}/cal$ and $-1.536 {}^\circ C \cdot cm^2 \cdot sec/cal$ respectively. If a sensor has the mean slope and intercept, the computational error of the heat flux predicted by neglecting the intercept would drop to about 10% in 0.22 sec. Therefore, Eq. (A9) is significant only at the beginning of time. However, when $t < (intercept/slope)^2$, Eq. (A9) becomes:

$$CF \begin{cases} \geq 0 \quad and \quad < 0.5 \quad for\ positive\ intercept \\ < 0 \qquad\qquad\qquad for\ negative\ intercept \end{cases}$$

Practically CF can never be less than zero. Therefore, for the case of negative intercept, Eq. (A9) can only be used for $t > (intercept/slope)^2$, i.e. for time greater than the time lag. The prediction of heat flux for each sensor was corrected using its unique correction factor, CF.

SKIN MODEL

The model used was developed by Mehta and Wong from M.I.T. [A3]. The skin was modelled as consisting of three layers: the epidermis, the dermis and the subcutaneous tissue, each of uniform thickness as shown in Fig. A4a. The arteries and veins are assumed to be straight to the dermis-epidermis interface. The deepest subcutaneous layer is considered to be at the constant normal body temperature (37°C). The blood in the artery is assumed to enter at this temperature. As the blood travels outward from the isothermal core, part of it will leave the arteries through the capillaries to the veins and finally back to the isothermal core. In this model each of the three layers is assumed to have constant thermal properties. The blood perfusion rate is assumed to be constant within the lower two layers, but is zero within the epidermis. The skin can be considered opaque or diathermanous depending on the source of thermal radiation. Opaque skin ignores the effect of penetrating radiant heat flow, while the diathermanous skin model accounts for the penetration effects of thermal radiation.

In developing the energy balance equations for the three layers, Mehta and Wong further assumed that:

1. The heat transfer is a one-dimensional transient flow through the skin layers.
2. The outlet temperature of the blood from the capillaries to the veins equilibrates with the local tissue temperature because of the large surface-to-volume ratio and relatively long time of residence of blood in the capillaries.
3. Heat transfer between the larger blood vessels (arteries and veins) and the tissue is negligible. The temperature of the arterial blood, unlike the blood temperature in the veins, is independent of x and equal to the normal body temperature.
4. Transmission of radiation through diathermanous skin obeys the Beer-Lamber law with one absorption coefficient applying for the epidermal layer, and another for the deeper tissue. Absorption of radiation by the blood is negligible.

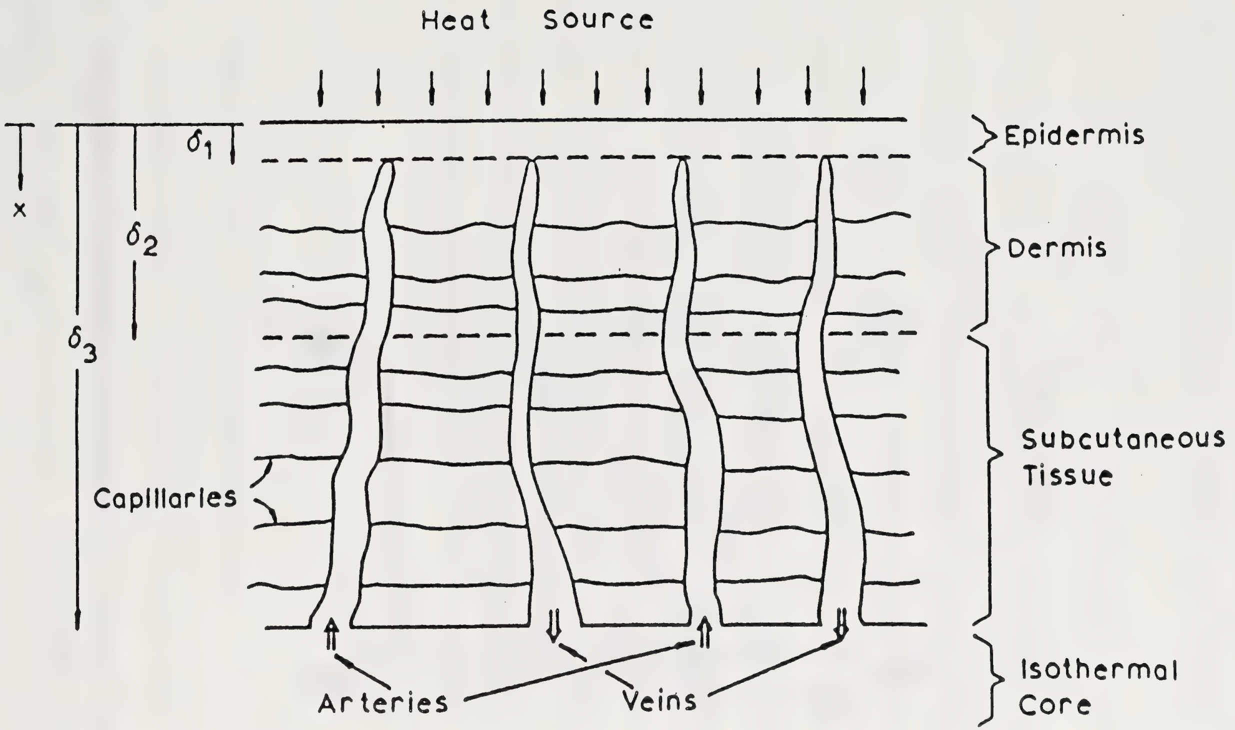

Fig. A4a The skin model

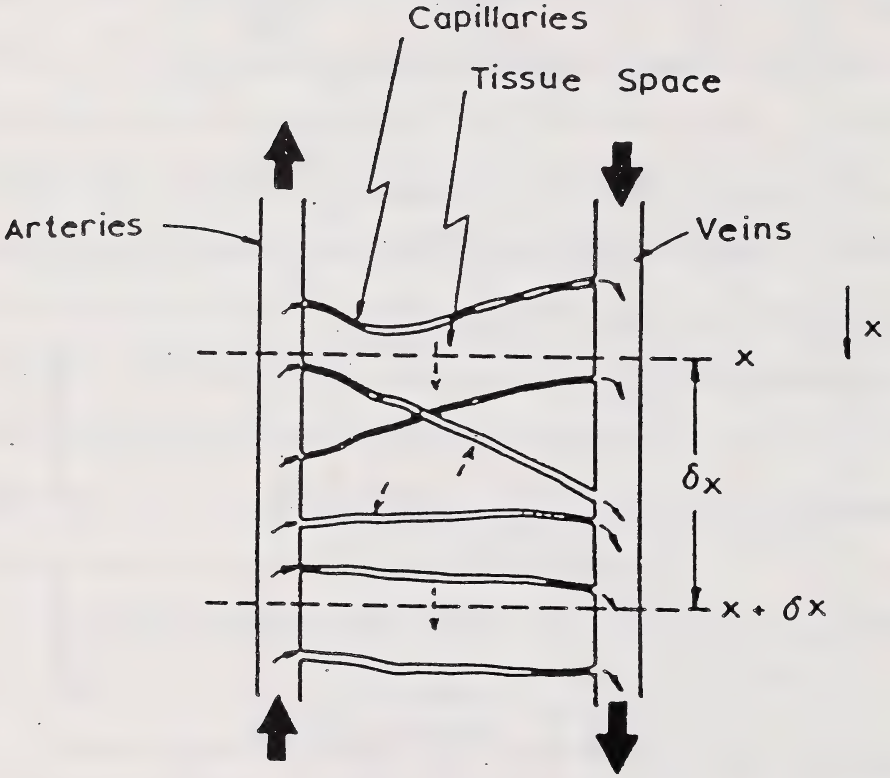

Fig. A4b A volume element of skin indicating the blood flow (solid arrows) and heat transfer (dotted arrows)

On the basis of the above assumptions, the transient flow of heat through a volume tissue element as shown in Fig. A4b can be described by the following equation:

$$C\rho \frac{\partial T}{\partial t} = k\frac{\partial^2 T}{\partial x^2} - (C\rho)_b G(T - T_b) + qf \qquad \text{(A10)}$$

The left hand side of Eq. (A10) represents the rate of increase of energy content of the tissue in which $C\rho$ is the volumetric heat capacity in cal/cm$^3\cdot$°C and T is the tissue temperature. The first term on the right side represents the conductive heat gain within the tissue, where k is the thermal conductivity in cal/cm· sec·°C. The second term on the right is the heat transfer from the tissue to the capillaries in which $(C\rho)_b$ denotes the volumetric heat capacity of the blood, G is the blood perfusion rate in cc/sec per cc of tissue volume and T_b is the perfusing blood temperature (i.e. the arterial blood temperature, but assumed to be at 37°C, the internal body temperature). The last term represents the absorption of penetrating radiation by the tissue in which q is the absorbed radiation at the surface in cal/sec· cm^2 and f denotes the energy attenuation functions which are defined as follows:

$$\begin{aligned} f = f(x) &= \gamma_1 e^{-\gamma_1 x}, && 0 \le x < \delta_1 \\ &= \gamma_2 e^{-\gamma_1 \delta_1} e^{-\gamma_2 (x - \delta_1)}, && x \ge \delta_1 \end{aligned} \qquad \text{(A11)}$$

where γ_1 = absorption coefficient for the epidermal layer, cm^{-1}

γ_2 = absorption coefficient for the dermal and subcutaneous layers, cm^{-1}

δ_1 = thickness of epidermis, cm.

Equation (A10) can be solved for the three layers. For opaque skin, the last term in Eq. (A10) is omitted. In the epidermal layer, the blood perfusion G is zero because of its nonvascularity. The initial and boundary conditions to be satisfied are:

(i) $t = 0,\ T = T_o(x)$ = an initial temperature profile

(ii) $t > 0,\ x = 0,$

$$-k_1 \frac{\partial T}{\partial x} = q(t) - h(T - T_\infty) \quad \text{for opaque skin}$$

or $$k_1 \frac{\partial T}{\partial x} = h(T - T_\infty) \quad \text{for diathermanous skin}$$

where k_1 = thermal conductivity of the epidermis, cal/sec· cm·°C

$q(t)$= radiation heat flux at the surface, cal/cm^2· sec

h = overall surface heat loss coefficient, cal/cm^2· sec·°C

T_∞ = ambient temperature, °C

(iii) $t > 0,\ x = \delta_3,\ T = T_b$

where δ_3 = distance of the deepest subcutaneous layer from the surface, cm

T_b = normal body temperature, °C

(iv) Continuity of temperature and heat flux at the two interfaces at all times.

To solve Eq. (A10) numerically, a non-uniform grid system was devised with fine grid near the skin surface and the two interfaces, which was stretched to a coarse size in the regions where the temperature gradients are smaller. This grid system is shown in Fig. A5 and described in the following equations.

$$\Delta x_i = x_{i+1} - x_i = \begin{cases} \Delta x_1 R_1^{(i-1)} & \text{for } i = 1,2,3,\dots,N1-1 \\ \Delta x_1 & \text{for } i = N1 \\ \Delta x_{N1+1} R_2^{(i-N1-1)} & \text{for } i = N1+1,\ N1+2,\dots,N1+N2-1 \\ \Delta x_{N1+1} & \text{for } i = N1+N2 \\ \Delta x_{N1+N2+1} R_3^{(i-N1-N2-1)} & \text{for } i = N1+N2+1,\dots,N1+N2+N3 \end{cases} \qquad \text{(A12)}$$

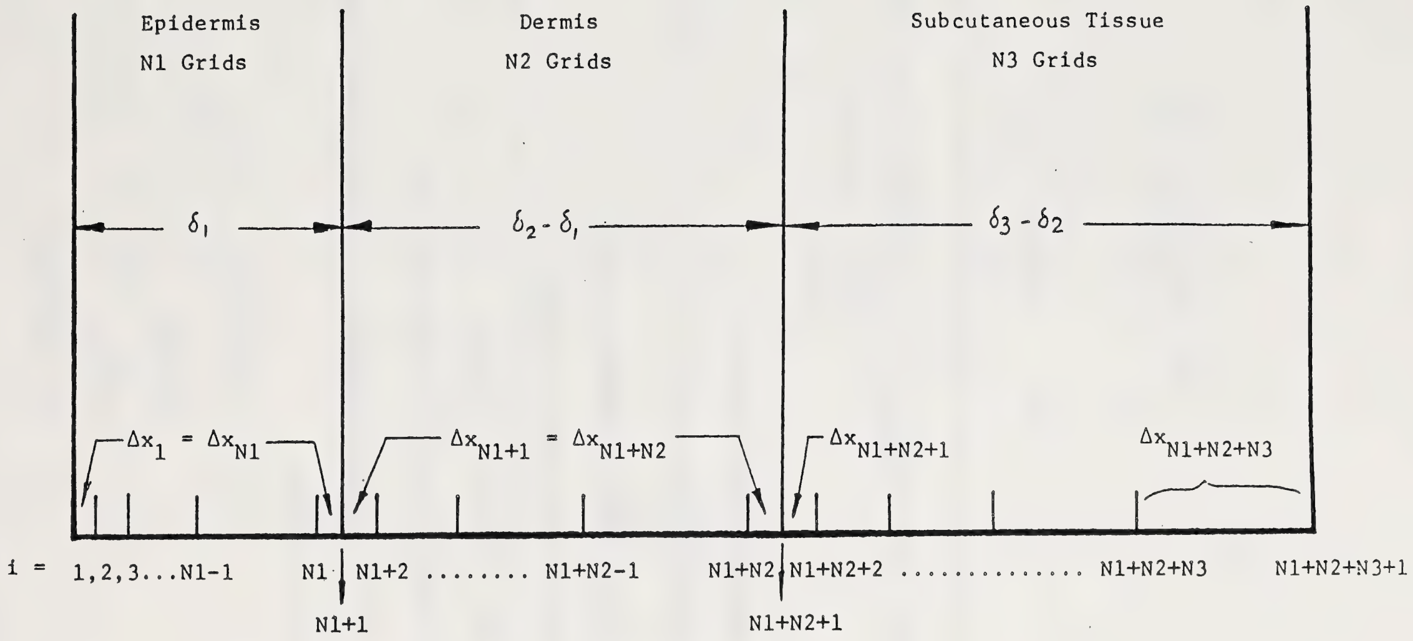

Fig. A5 A nonlinear finite difference grid for the skin model

where

$$\Delta x_1 = \frac{\delta_1}{1 + \sum_{i=1}^{N1-1} R_1^{(i-1)}}$$

$$\Delta x_{N1+1} = \frac{\delta_2 - \delta_1}{1 + \sum_{i=N1+1}^{N1+N2-1} R_2^{(i-N1-1)}}$$

$$\Delta x_{N1+N2+1} = \frac{\delta_3 - \delta_2}{\sum_{i=N1+N2+1}^{N1+N2+N3} R_3^{(i-N1-N2-1)}}$$

N1 = number of grids in epidermis

N2 = number of grids in dermis

N3 = number of grids in subcutaneous tissue

R_1 = axial stretching ratio for epidermis

R_2 = axial stretching ratio for dermis

R_3 = axial stretching ratio for subcutaneous tissue

Also, to solve Eq. (A10) numerically, it is more convenient to express Eq.(A10) in a dimensionless form by defining:

$$\theta = (T - T_b)/T_b \qquad \text{(A13)}$$

$$X = x/\delta_1 \qquad \text{(A14)}$$

$$\tau = t/t_o \qquad \text{(A15)}$$

$$\Phi = (t_o/C\rho T_b)qf \qquad \text{(A16)}$$

where t_o = exposure time.

Thus, Eq. (A10) becomes:

$$\frac{\partial \theta}{\partial \tau} = \beta \frac{\partial^2 \theta}{\partial X^2} - \lambda \theta + \Phi \qquad \text{(A17)}$$

where $\beta = \frac{k}{C\rho} \frac{t_o}{\delta_1^2}, \quad \lambda = \frac{(C\rho)_b}{C\rho} G t_o.$

Based on the concept of the Crank-Nicholson Implicit Method, each term in Eq. (A17) is written in a finite difference form at the point (i, j+½) in the time-distance coordinate plane as follows:

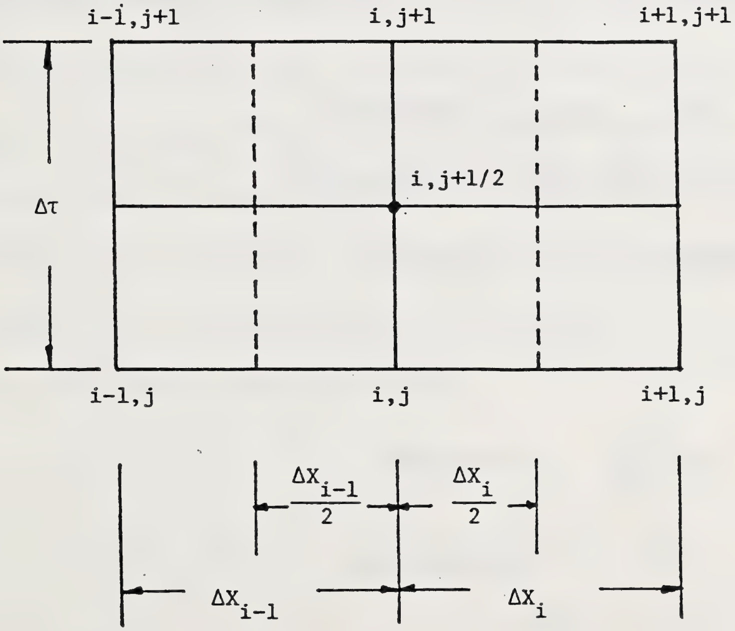

$$\frac{\partial\theta}{\partial\tau}\Big|_{i,j+½} = \frac{\theta_{i,j+1}-\theta_{i,j}}{\Delta\tau}$$

$$\beta\frac{\partial^2\theta}{\partial X^2}\Big|_{i,j+½} = \frac{\beta_i}{\Delta X_i+\Delta X_{i-1}}\left[\left(\frac{\theta_{i+1,j}-\theta_{i,j}}{\Delta X_i}-\frac{\theta_{i,j}-\theta_{i-1,j}}{\Delta X_{i-1}}\right)+\left(\frac{\theta_{i+1,j+1}-\theta_{i,j+1}}{\Delta X_i}-\frac{\theta_{i,j+1}-\theta_{i-1,j+1}}{\Delta X_{i-1}}\right)\right].$$

$$\lambda\theta\big|_{i,j+½} = \frac{\lambda_i}{2}\left[\theta_{i,j}+\theta_{i,j+1}\right]$$

$$\Phi_{i,j+½} = \frac{1}{2}\left[\Phi_{i,j}+\Phi_{i,j+1}\right]$$

where the subscripts i and j denote the points in coordinates X (or x) and τ (or t) respectively, and start at one.

The dimensionless finite different form of the initial and boundary conditions can be expressed as:

(i) $\theta_{i,1} = (T_{i,1} - T_b)/T_b$ $\quad i = 1, 2, ..., N1+N2+N3+1$ (A18)

where $T_{i,1} = T_o(x_i)$ = the initial temperature profile

(ii) $\frac{\theta_{2,j}-\theta_{o,j}}{2\Delta X_1} = H[\theta_{1,j} - \theta_\infty] - \phi_j,$ $\quad j = 2, 3, 4, ...$ (A19)

where $H = h\delta_1/k_1$

$\phi_j = \frac{\delta_1 q_j}{k_1 T_b}$ for opaque skin

$= 0$ for diathermanous skin

$\theta_\infty = (T_\infty - T_b)/T_b$

$\theta_{o,j}$ = fictitious dimensionless temperature

(iii) $\theta_{N1+N2+N3+1,j} = 0$ $\quad j = 2, 3, 4 ...$ (A20)

(iv)
$$\frac{\theta_{N1+1,j}-\theta_{N1,j}}{\Delta X_{N1}} = \frac{k_2}{k_1}\frac{\theta_{N1+2,j}-\theta_{N1+1,j}}{\Delta X_{N1+1}} \tag{A21}$$

$$\frac{\theta_{N1+N2+1,j}-\theta_{N1+N2,j}}{\Delta X_{N1+N2}} = \frac{k_3}{k_2}\frac{\theta_{N1+N2+2,j}-\theta_{N1+N2+1,j}}{\Delta X_{N1+N2+1}} \tag{A22}$$

j = 2, 3, 4 ...

Where k_1, k_2 and k_3 are the thermal conductivities of the epidermis, dermis and subcutaneous tissue, respectively.

Since the temperature at the (N1+N2+N3+1)-th point is given in Eq. (A20) and the fictitious temperature at the 0-th point is given in Eq. (A19), rearrangements of the finite difference form of Eq. (A17) for i = 1,2, ..., N1, N1+2, ..., N1+N2, N1+N2+2, ..., N1+N2+N3; Eq. (A21) for i = N1+1 and Eq. (A22) for i = N1+N2+1 provide (N1+N2+N3) coupled algebraic equations for the (N1+N2+N3) unknown nodal-point temperature at time j+1. The matrix form of these equations is given in Eq. (A23). The elements of the tri-diagonal matrix of Eq. (A23) are defined in Eqs. (A23a), (A23b) and (A23c). While the elements in the vector matrix on the right hand side of Eq. (A23) are given in Eq. (A23d).

$$\begin{bmatrix}
b_1 & c_1 & & & & & & & \\
a_2 & b_2 & c_2 & & & & & & \\
 & \ddots & \ddots & \ddots & & & & & \\
 & a_{N1} & b_{N1} & c_{N1} & & & & & \\
 & & a_{N1+1} & b_{N1+1} & c_{N1+1} & & & & \\
 & & & \ddots & \ddots & \ddots & & & \\
 & & & a_{N1+N2} & b_{N1+N2} & c_{N1+N2} & & & \\
 & & & & a_{N1+N2+1} & b_{N1+N2+1} & c_{N1+N2+1} & & \\
 & & & & & \ddots & \ddots & \ddots & \\
 & & & & & & a_{N1+N2+N3-1} & b_{N1+N2+N3-1} & c_{N1+N2+N3-1} \\
 & & & & & & & a_{N1+N2+N3} & b_{N1+N2+N3}
\end{bmatrix}
\begin{bmatrix}
\theta_{1,j+1} \\
\theta_{2,j+1} \\
\vdots \\
\theta_{N1,j+1} \\
\theta_{N1+1,j+1} \\
\vdots \\
\theta_{N1+N2,j+1} \\
\theta_{N1+N2+1,j+1} \\
\vdots \\
\theta_{N1+N2+N3-1,j+1} \\
\theta_{N1+N2+N3,j+1}
\end{bmatrix}
=
\begin{bmatrix}
D_{1,j} \\
D_{2,j} \\
\vdots \\
D_{N1,j} \\
D_{N1+1,j} \\
\vdots \\
D_{N1+N2,j} \\
D_{N1+N2+1,j} \\
\vdots \\
D_{N1+N2+N3-1,j} \\
D_{N1+N2+N3,j}
\end{bmatrix}
\quad (A23)$$

$$a_i = \begin{cases} \alpha_1 \dfrac{\Delta t}{\Delta x_1^2} & for\ i = 1 \\ -2\ \alpha_1 \dfrac{\Delta t}{\Delta x_{i-1}(\Delta x_i + \Delta x_{i-1})} & for\ i = 2,3,\ldots,N1 \\ 1 & for\ i = N1+1 \\ -2\ \alpha_2 \dfrac{\Delta t}{\Delta x_{i-1}(\Delta x_i + \Delta x_{i-1})} & for\ i = N1+2, N1+3,\ldots,N1+N2 \\ 1 & for\ i = N1+N2+1 \\ -2\ \alpha_3 \dfrac{\Delta t}{\Delta x_{i-1}(\Delta x_i + \Delta x_{i-1})} & for\ i = N1+N2+2, N1+N2+3,\ldots,N1+N2+N3 \end{cases} \tag{A23a}$$

$$b_i = \begin{cases} 1 + a_1 + \dfrac{\Lambda_1}{2} + \eta & for\ i = 1 \\ 2 + 2\alpha_1 \dfrac{\Delta t}{\Delta x_i \Delta x_{i-1}} + \Lambda_1 & for\ i = 2,3,\ldots,N1 \\ -\left(\dfrac{k_2}{k_1} \dfrac{\Delta x_{N1}}{\Delta x_{N1+1}} + 1\right) & for\ i = N1+1 \\ 2 + 2\alpha_2 \dfrac{\Delta t}{\Delta x_i \Delta x_{i-1}} + \Lambda_2 & for\ i = N1+2, N1+3,\ldots,N1+N2 \\ -\left(\dfrac{k_3}{k_2} \dfrac{\Delta x_{N1+N2}}{\Delta x_{N1+N2+1}} + 1\right) & for\ i = N1+N2+1 \\ 2 + 2\alpha_3 \dfrac{\Delta t}{\Delta x_i \Delta x_{i-1}} + \Lambda_3 & for\ i = N1+N2+1, N1+N2+2,\ldots,N1+N2+N3 \end{cases} \tag{A23b}$$

$$c_i = \begin{cases} -a_1 & \mathit{for}\ i = 1 \\ -2\alpha_1 \dfrac{\Delta t}{\Delta x_i(\Delta x_i + \Delta x_{i-1})} & \mathit{for}\ i = 2,3,\ldots,N1 \\ \dfrac{k_2}{k_1}\,\dfrac{\Delta x_{N1}}{\Delta x_{N1+1}} & \mathit{for}\ i = N1+1 \\ -2\alpha_2 \dfrac{\Delta t}{\Delta x_i(\Delta x_i + \Delta x_{i-1})} & \mathit{for}\ i = N1+2, N1+3, \ldots, N1+N2 \\ \dfrac{k_3}{k_2}\,\dfrac{\Delta x_{N1+N2}}{\Delta x_{N1+N2+1}} & \mathit{for}\ i = N1+N2+1 \\ -2\alpha_3 \dfrac{\Delta t}{\Delta x_i(\Delta x_i + \Delta x_{i-1})} & \mathit{for}\ i = N1+N2+2, N1+N2+3, \ldots, N1+N2+N3 \end{cases} \tag{A23c}$$

$$D_{i,j} = \begin{cases} (2-b_1)\theta_{1,j} + a_1\theta_{2,j} + 2\eta\theta_\infty + PHI(j) + \frac{1}{2}F_1(1,j) \\ \qquad\qquad\qquad\qquad \mathit{for}\ i = 1 \\ -a_i\theta_{i-1,j} + [4-b_i]\theta_{i,j} - c_i\theta_{i+1,j} + F_1(i,j) \\ \qquad\qquad\qquad\qquad \mathit{for}\ i = 2,3,\ldots,N1 \\ 0 \qquad\qquad\qquad\qquad \mathit{for}\ i = N1+1 \\ -a_i\theta_{i-1,j} + [4-b_i]\theta_{i,j} - c_i\theta_{i+1,j} + F_2(i,j) \\ \qquad\qquad\qquad\qquad \mathit{for}\ i = N1+2, N1+3,\ldots,N1+N2 \\ 0 \qquad\qquad\qquad\qquad \mathit{for}\ i = N1+N2+1 \\ -a_i\theta_{i-1,j} + [4-b_i]\theta_{i,j} - c_i\theta_{i+1j} + F_3(i,j) \\ \qquad\qquad\qquad\qquad \mathit{for}\ i = N1+N2+2, N1+N2+3,\ldots,N1+N2+N3-1 \\ -a_{N1+N2+N3}\theta_{N1+N2+N3-1,j} + [4-b_{N1+N2+N3}]\,\theta_{N1+N2+N3,j} - c_{N1+N2+N3}(\theta_{N1+N2+N3+1,j} \\ \quad +\theta_{N1+N2+N3+1,j+1}) + F_3(N1+N2+N3,j) \qquad \mathit{for}\ i = N1+N2+N3 \end{cases} \tag{A23d}$$

where

$$\alpha_k = \left(\frac{k}{C\rho}\right)_k$$

$$\Lambda_k = \left(\frac{G}{C\rho}\right)_k (C\rho)_b \Delta t$$

$$\eta = \frac{h\Delta t}{(C\rho)_1 \Delta x_1}$$

$$PHI(j) = \begin{cases} \dfrac{\Delta t}{(C\rho)_1 \Delta x_1 T_b} (q_j + q_{j+1}) & \textit{for opaque skin} \\ 0 & \textit{for diathermanous skin} \end{cases}$$

$$F_k(i,j) = \begin{cases} \dfrac{\Delta t\, f_i}{(C\rho)_k T_b} (q_j + q_{j+1}) & \textit{for diathermanous skin} \\ 0 & \textit{for opaque skin} \end{cases}$$

and f_i is given in Eq. (A11) which is:

$$f_i = \begin{cases} \gamma_1\, e^{-\gamma_1 x_i} & \textit{for } 1 \le i < N1+1 \\ \gamma_2\, e^{-\gamma_1 \delta_1}\, e^{-\gamma_2 (x_i - \delta_1)} & \textit{for } i \ge N1+1 \end{cases}$$

The subscript k for α, ∧ and F denotes the skin layer in the following manner:

$$k = \begin{cases} 1 & \textit{for epidermis} \\ 2 & \textit{for dermis} \\ 3 & \textit{for subcutaneous tissue} \end{cases}$$

and the subscript b denotes the blood. Also, Δx and Δt in the above equations are no longer the dimensionless ΔX and Δτ, although Eq. (A23) is a set of non-dimensional equations.

Equation (A23) can be solved for the dimensionless temperatures at time j+1 using the Thomas-Algorithm, provided that the temperatures at time j are known. In this model, the initial temperature gradient is assumed to be linear from the skin surface (32.5°C) to the deepest portion of the subcutaneous region (37°C). Then, the new temperatures at j = 2 can be calculated. Repeatedly, the temperatures for each time-step following are found. The time-step employed in this model is 1 second. The numbers of grids, the stretching ratios, the thermal properties, the blood perfusion rates and the thicknesses for the epidermal, dermal and subcutaneous layers used in this model are summarized in Table A2. The surface heat loss coefficient, h, given in [A3] is 4.5×10^{-4} cal/cm^2· sec·°C. If the skin surface is covered with garments, it is suggested to ignore the heat loss coefficient. Furthermore, the emissivity of human skin is assumed to be one.

TABLE A2 Parameters Used in the Model

Parameters	Epidermis	Dermis	Subcutaneous Tissue	Blood
Number of Grid	6	24	15	-
Stretching Ratio	1.25	1.25	1.25	-
Overall Thickness of Layer (cm)	0.008	0.2	1.0	-
Conductivity, k (cal/cm·°C· sec)	6.1×10^{-4}	12.5×10^{-4}	4.0×10^{-4}	-
Volumetric cap. Cρ(cal/cm^3·°C)	1.032	0.924	0.660	0.954
Blood perfusion rate, G (cm^3/sec per cm^3 of tissue)	0.0	0.00125	0.00125	-
Absorption coefficient, γ (cm^{-1})	180.0	7.5	7.5	-

In order to test the computational accuracy of the model and the effects of the numbers of grids, the stretching ratios and the time-step, a simplified problem was studied. This problem considers an opaque skin with a semi-infinite boundary. A constant heat flux of 0.282 cal/sec· cm^2 and a uniform initial temperature of 32.5°C were used. The thermal properties of the skin were simplified to:

$$k_1 = k_2 = k_3 = 8.83 \times 10^{-4} \text{ cal/cm}\cdot{}^\circ\text{C}\cdot \text{sec}$$

$$(C\rho)_1 = (C\rho)_2 = (C\rho)_3 = 0.924 \text{ cal/cm}^3\cdot{}^\circ\text{C}$$

$$G_1 = G_2 = G_3 = 0$$

and the surface heat loss coefficient was set to zero. Thus an analytical solution for this simple problem can be obtained from Eq. (A7). The analytical solution was then compared with the finite difference solutions for various numbers of grids, stretching ratios and time-steps. The different sets of parameters used are defined in Table A3, and the results of the temperature at 0.008 cm for the different cases are shown in Table A4.

Comparison of Cases a, e and k in Table A4 indicates that for the range of grid sizes studied, increase in number of grids does not obviously improve the accuracy. However, change of the stretching ratios does change the finite difference solution. As indicated in Cases e to i, the finite difference solution slightly approaches the analytical solution when the stretching ratios are increased until they reach a value of about 1.3, above which accuracy decreases. A value of 1.25 for the stretching ratios appears to work satisfactorily for almost all cases (Cases b, c, g, j, l, m and n). Also, Cases b, c, d, e, l and m indicate that decreasing the time-step by half does not show obvious improvement on the accuracy for the heat flux of 0.282 cal/cm^2· sec.

According to the above analysis, the values of the numbers of grids and the stretching ratios shown in Table A2, and a time-step of 1 sec appear to be appropriate for solving this type of transient temperature problems. The finite difference approach developed in this section is useful for solving the skin model, and the computational accuracy is reasonably good.

TABLE A3 The numbers of grids, stretching ratios and time-steps used for testing the model

Case	N1	N2	N3	R1	R2	R3	Δt (sec)
a	50	50	20	1	1	1	1
b	50	50	20	1.25	1.25	1.25	1
c	50	50	20	1.25	1.25	1.25	0.5
d	12	36	24	1	1	1	0.5
e	12	36	24	1	1	1	1
f	12	36	24	1.1	1.1	1.1	1
g	12	36	24	1.25	1.25	1.25	1
h	12	36	24	1.5	1.5	1.5	1
i	12	36	24	1.65	1.65	1.65	1
j	8	28	18	1.25	1.25	1.25	1
k	6	24	15	1	1	1	1
l	6	24	15	1.25	1.25	1.25	1
m	6	24	15	1.25	1.25	1.25	0.5
n	2	16	9	1.25	1.25	1.25	1

TABLE A4 Comparison of the Finite Difference and Analytical Solutions for A Transient Temperature Problem

Time (sec)	Finite Difference Solutions (Temperatures at 0.008 cm, °C)														Analytical Solution Temp. at 0.008 cm (°C)
	Cases														
	a	b	c	d	e	f	g	h	i	j	k	l	m	n	
0	32.5	32.5	32.5	32.5	32.5	32.5	32.5	32.5	32.5	32.5	32.5	32.5	32.5	32.5	32.5
1	42.9	42.0	41.5	42.1	43.3	42.4	42.2	42.3	41.9	42.3	43.9	42.4	41.5	43.2	41.27
2	46.1	45.6	46.1	46.8	46.4	45.8	45.7	46.0	42.3	45.8	46.7	45.8	46.1	46.2	45.83
3	50.1	49.1	49.7	50.4	50.4	49.6	49.4	50.1	44.1	49.5	51.0	49.6	49.6	50.3	49.35
4	52.9	52.1	52.6	53.4	53.2	52.5	52.4	53.3	47.2	52.4	53.6	52.5	52.6	53.0	52.32
5	55.5	54.4	55.4	56.0	55.8	55.0	54.8	56.1	46.4	54.9	56.3	55.0	55.2	55.7	54.94
6	58.0	57.3	57.9	58.3	58.3	57.6	57.4	59.0	49.9	57.5	58.8	57.6	57.5	58.1	57.31
7	60.0	58.7	60.3	60.5	60.3	59.5	59.3	61.2	48.8	59.4	60.8	59.4	59.7	60.2	59.49
8	62.3	60.9	62.6	62.5	62.6	61.8	61.6	63.7	56.4	61.7	63.1	61.8	61.7	62.4	61.52
9	63.9	62.5	64.8	64.4	64.2	63.4	63.2	65.8	52.9	63.3	64.7	63.4	63.6	64.1	63.43
10	66.0	64.3	66.8	66.3	66.3	65.6	65.3	68.3	58.4	65.4	66.9	65.5	65.4	66.1	65.23

BURN MODEL

Burn damage is assumed to follow a first order reaction rate process [A1], the Arrhenius equation:

$$\Omega = p \int_{o}^{t} e^{\frac{-\Delta E}{RT}}\, dt$$

where:

Ω = a quantitative measure of burn damage at the basal layer or at any depths in the dermis

P = frequency factor, $\sec^{-1}$

$\Delta E/R$ = activation energy (ΔE in cal/mole) divided by the gas constant (R in cal/mole· K)

T = absolute temperature at the basal layer or at any depths in the dermis, K

t = total time for which T is above 317.15 K (44°C), the minimum injurious temp.

Several burn criteria from the literature are available for use with this model. The differences in the criteria are mainly the different values of P and $\Delta E/R$. These criteria include:

1. Henrique's Burn Criterion [A1]

Based on experiments of epidermal burns and extended to predict dermal burn damage. Considers only the damage incurred during the heating up period of a burn.

$$P = 3.1 \times 10^{98} \sec^{-1}$$
$$\Delta E/R = 75{,}000.0\ K$$

2. Stoll's Burn Criteria [A2]

Based on experimental epidermal burn data and extended to predict dermal burn damage. It considers the total damage incurred during both the heating and cooling periods.

$$\left.\begin{array}{l} P = 2.185 \times 10^{124}\ \mathrm{sec}^{-1} \\ \Delta E/R = 93{,}534.9\ K \end{array}\right\} \quad \textit{for } T < 50^{\circ}C$$

$$\left.\begin{array}{l} P = 1.823 \times 10^{51}\ \mathrm{sec}^{-1} \\ \Delta E/R = 39{,}109.8\ K \end{array}\right\} \quad \textit{for } T \geq 50^{\circ}C$$

3. M.I.T.'s Burn Criteria [A3]

Based on both epidermal and dermal experimental burn data. It accounts for damage during both heating and cooling periods and includes body fluid convection effects.

$$\left.\begin{array}{l} P = 1.43 \times 10^{72}\ \mathrm{sec}^{-1} \\ \Delta E/R = 55{,}387.71\ K \end{array}\right\} \quad \textit{for epidermis}$$

$$\left.\begin{array}{l} P = 2.86 \times 10^{69}\ \mathrm{sec}^{-1} \\ \Delta E/R = 55{,}387.71\ K \end{array}\right\} \quad \textit{for dermis}$$

4. Takata's Criteria [A4]

These criteria were developed for dermal burn damage assessment only.

$$\left.\begin{array}{l} P = 4.32 \times 10^{64}\ \mathrm{sec}^{-1} \\ \Delta E/R = 50{,}000\ K \end{array}\right\} \quad \textit{for } T < 50^{\circ}C$$

$$\left.\begin{array}{l} P = 9.39 \times 10^{104}\ \mathrm{sec}^{-1} \\ \Delta E/R = 80{,}000\ K \end{array}\right\} \quad \textit{for } T \geq 50^{\circ}C$$

Morse, H. et al. [A5] recommended that the Stoll criteria for epidermal burn prediction and the Takata criteria for dermal damage be combined for the best prediction for cutaneous burns. This study will use this recommendation.

In evaluation the models for this study, the trapezoidal rule is employed to integrate the Arrhenius equation numerically to obtain the damage function Ω. Once Ω is found, the degree of burn is determined according to the following table.

Assessment of Degree Burn

$\Omega \leq 0.5$ at 0.008 cm	No burn damage
$0.5 < \Omega < 1.0$ at 0.008 cm	1st degree burn
$\Omega \geq 1.0$ at 0.008 cm and $\Omega < 1.0$ at 0.2 cm	2nd degree burn
$\Omega \geq 1.0$ at 0.2 cm	3rd degree burn

and the depth of irreversible damage is defined as the depth at which $\Omega = 1$.

Since the combined criteria of Stoll and Takata have been proven to give the best prediction of cutaneous burns, these criteria were used in the following analysis to test the combined accuracy of the skin and burn models. Different constant heat fluxes were input to the program. The time to 2nd degree burn (i.e. the time at which Ω at 0.008 cm reaches one) was then predicted by the program for each of the input heat flux. Three different versions of the program were studied and the results were compared with the measurements from Stoll and Chianta [A9]. The differences between the three versions are shown in Table A5 and the results are plotted on log-log coordinates in Fig. A6.

In Table A5 the conductivities used in the old version and New version 1 were obtained from Henriques and Moritz [A10]. The conductivities used in New version 2 are the averages of those within the three individual layers presented in Elkins and Thompson [A8]. As seen in Fig. A6, New version 2 predicts the best results of the occurrence of 2nd degree burn (or blistering).

TABLE A5 The Parameters Used in the Three Versions

	k_1	k_2	k_3	N1	N2	N3	R1	R2	R3
		(cal/cm sec °C)							
Old version	5×10^{-4}	8.83×10^{-4}	3.83×10^{-4}	12	36	24	1	1	1
New version 1	5×10^{-4}	8.83×10^{-4}	3.83×10^{-4}	6	24	15	1.25	1.25	1.25
New version 2	6.1×10^{-4}	12.5×10^{-4}	4.0×10^{-4}	6	24	15	1.25	1.25	1.25

Since there is no similar information available from the literature about the 3rd degree burn, prediction of 3rd degree burn cannot be justified.

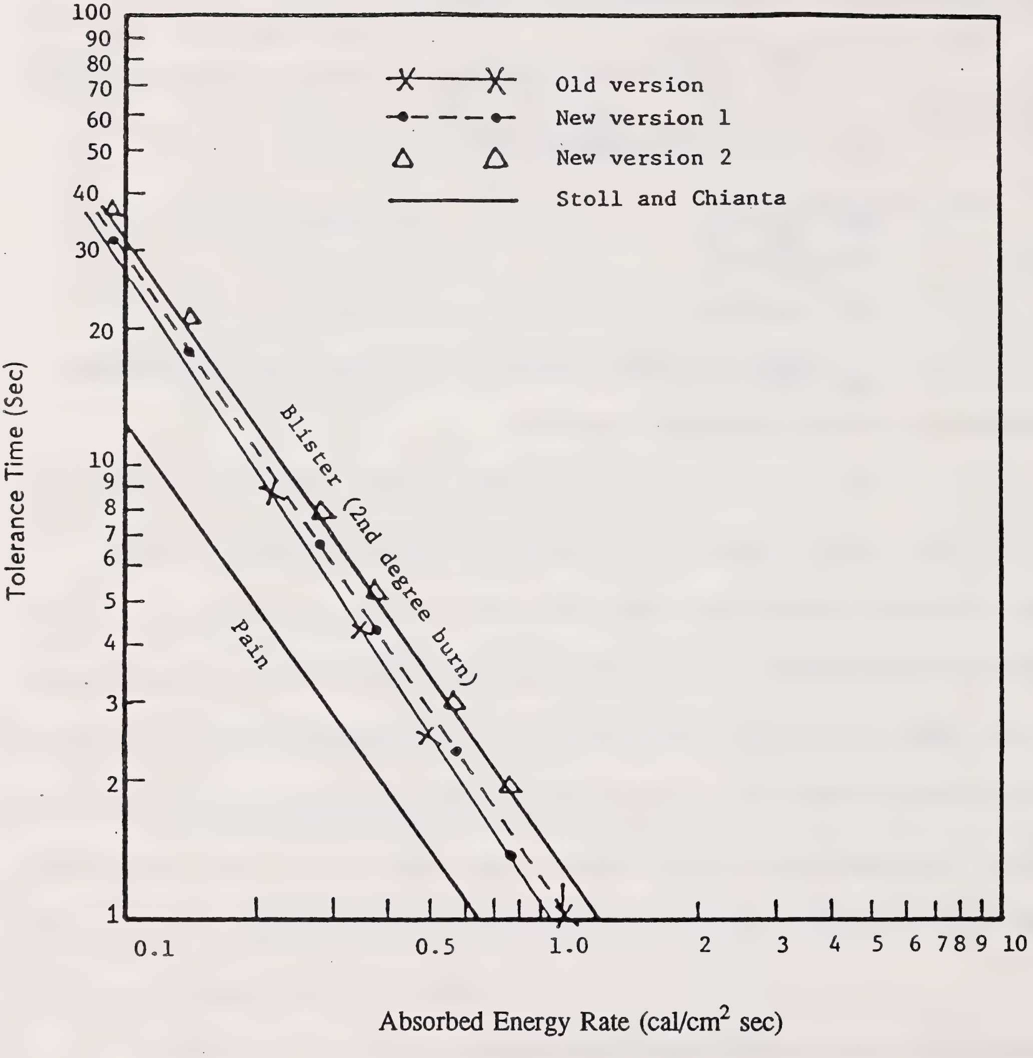

Fig. A6 Measured and predicted human skin tolerance time to absorbed energy rate

REFERENCES

[A1] Henriques, F.C., "Studies of Thermal Injury: V. The Predictability and the Significance of Thermally Induced Rate Processes Leading to Irreversible Epidermal Injury", Archives of Pathology, Vol. 43, p. 489, 1947.

[A2] Stoll, A.M. and Greene, L.C., "Relationship Between Pain and Tissue Damage Due to Thermal Radiation", Journal of Applied Physiology, Vol. 14, p. 373, 1959.

[A3] Mehta, A.K. and Wong, F., "Measurement of Flammability and Burn Potential of Fabrics", Fuels Research Laboratory, M.I.T. Summary Report DSR 73884, Feb. 15, 1973.

[A4] Takata, A.N., Rouse, J. and Stanley, T., "Thermal Analysis Program", I.I.T. Research Institute Report, IITRI-J6286, Feb. 1973.

[A5] Morse, H., Tickner, G. and Brown, R., "Burn Damage and Burn Depth Criteria", Aerotherm Report TN-75-26, Jan. 1975.

[A6] Buettner, K., "Effects of Extreme Heat and Cold on Human Skin. I. Analysis of Temperature Changes Caused by Different Kinds of Heat Application", Journal of Applied Physiology, Vol. 3, p. 691, 1951.

[A7] Monette, R.C., "Measurement of Thermal Conductivity of a Composite Material", National Fire Laboratory, National Research Council of Canada, Report No. CR-6322.1, November 27, 1990.

[A8] Elkins, W. and Thompson, J.G., "Instrumentated Thermal Mannikin", Aerotherm Division/Acurex Corporation, Final Report AD-781176, January, 1973.

[A9] Stoll, A.M. and Chianta, M.A., "Method and Rating System for Evaluation of Thermal Protection", Aerospace Medicine, Vol. 40, p. 1232, 1969.

[A10] Henriques, F.C. and Moritz, A.R., "Studies of Thermal Injury: I. The Conduction of Heat to and Through Skin and the Temperatures Attained Therein. A Theoretical and an Experimental Investigation", American Journal of Pathology, Vol. 23, p. 531, 1947.

LIBRARY AND ARCHIVES CANADA
Bibliothèque et Archives Canada
3 3286 53882365 5